Available online at www.sciencedirect.com
ScienceDirect
Journal of Asian Earth Sciences 29 (2007) 41–61
Journal of Asian Earth Sciences
www.elsevier.com/locate/jaes

Ultrahigh-temperature mafic granulites from Panrimalai, south India: Constraints from phase equilibria and thermobarometry

D. Prakash [a,*], M. Arima [b], A. Mohan [a]

[a] Department of Geology, Banaras Hindu University, Varanasi 221005, India
[b] Geological Institute, Yokohama National University, 79-7 Tokiwadai, Hodogaya-ku, Yokohama 240-8501, Japan

Received 5 April 2005; received in revised form 1 November 2005; accepted 5 January 2006

Abstract

The Panrimalai area constitutes part of the granulite-facies rocks of the Madurai block in the Southern Granulite Terrain (SGT), India. Garnet-bearing mafic granulites in Panrimalai occur as small enclaves within charnockite. The common stable assemblage during peak metamorphism contains hornblende, garnet, orthopyroxene, clinopyroxene, quartz and plagioclase. The resorption of garnet in various reaction textures and the development of spectacular orthopyroxene–plagioclase and hornblende–plagioclase symplectites characterize the subsequent stages of metamorphism. Application of multi-equilibrium calculation procedures for mineral core compositions of the early assemblage yields near peak conditions at ≥ 900 °C at 9 kbar. These estimates are the highest yet reported in mafic granulites from the Madurai block. The post-peak *P–T* path is constructed for the mafic granulites based on observed microstructural relations and thermobarometric results is characterized by a steep clockwise decompressional *P–T* segment from ≥ 9 to < 4.5 kbar. Constraints from model Nd ages provide evidence for Paleoproterozoic magmatism restricted to the Madurai block in the Southern Granulite Terrain. The early part of the crustal evolution of the Panrimalai granulites could be coeval with the Paleoproterozoic event. Subsequent development of symplectitic assemblages via near-isothermal decompression can be ascribed to a distinctly later tectonic event. Available U–Pb and Sm–Nd mineral dates suggest a widespread Pan-African tectonothermal event in the SGT. Given the general recognition of ultrahigh-temperature (UHT) and isothermal decompression (ITD) in Pan-African age metamorphism in the East-African–Antarctic Orogen (EAAO) , the Panrimalai UHT history is considered to be part of this record.
© 2006 Elsevier Ltd. All rights reserved.

Keywords: Garnet-bearing mafic granulites; Symplectite textures; Ultrahigh-temperature decompression; SGT; Thermobarometry; TWQ program

1. Introduction

Ultrahigh-temperature (UHT) regional metamorphism is defined as metamorphism in which crustal rocks are subjected to temperatures of 900–1100 °C at moderate pressures of 7–13 kbar (Harley, 1998). Reports of such UHT conditions are increasingly common in southern India (Ravindra Kumar and Chacko, 1994; Nandakumar and Harley, 2000). Strong evidence for UHT metamorphism is described from sapphirine-bearing granulites that occur at Perumalmalai (Raith et al., 1997), Usilampatti (Prakash and Arima, 2003) and Rajapalaiyam (Tateishi et al., 2004) localities in the Palni hill ranges. Panrimalai, well known for the occurrence of sapphirine granulites (Grew, 1984; Mohan and Windley, 1993), represents a portion of the granulite-facies terrain of the Palni hills in the Madurai block, southern India. Mafic granulites of the study area that preserve its metamorphic history in the form of reaction textures and symplectites have high potential to elucidate the conditions of HT/UHT metamorphism. These mafic granulites occur in several localities in the Southern Granulite Terrain (SGT) of India (Mohan et al., 1985; Ravindra Kumar and Chacko, 1994; Prakash, 1999a). *P–T* vectors indicating retrograde decompressive PT paths in HT/UHT granulites are prolific in mafic granulites from several Precambrian regional terrains of the world

* Corresponding author.
E-mail addresses: dprakash_vns@rediffmail.com (D. Prakash), arima@ed.ynu.ac.jp (M. Arima), amohanbhu@yahoo.com (A. Mohan).

1367-9120/$ - see front matter © 2006 Elsevier Ltd. All rights reserved.
doi:10.1016/j.jseaes.2006.01.002

including Eastern Ghats belt, Rauer Islands, Northern Labrador, Søstrene Island, Central Finland, Algeria, Germany and NE Greenland (Harley, 1988; Mengel and Rivers, 1991; Thost et al., 1991; Dasgupta et al., 1993; Brodie, 1995; Attoh, 1998; Zhao et al., 2000; Holtta and Paavola, 2000; Ouzegane et al., 2001; Rotzler and Romer, 2001; Jones and Escher, 2002; Bhowmik and Roy, 2003).

In the present communication, we describe spectacular textural features and mineral chemical data from garnet-bearing mafic granulites of the Panrimalai area. Based on phase equilibria and thermobarometric constraints, a UHT decompressional *P–T* path for the Panrimalai mafic granulites is proposed. We also address the implication of these UHT granulites in light of East Gondwana assembly.

2. Geological background

The Panrimalai area (77°45′E, 10°19′23″N to 77°50′30″E, 10°23′7″N) is an integral part of SGT and has elicited a good deal of interest on account of its interesting rock types and varied mineralogy. The study area, situated in the Palni hills of the Madurai block, lies

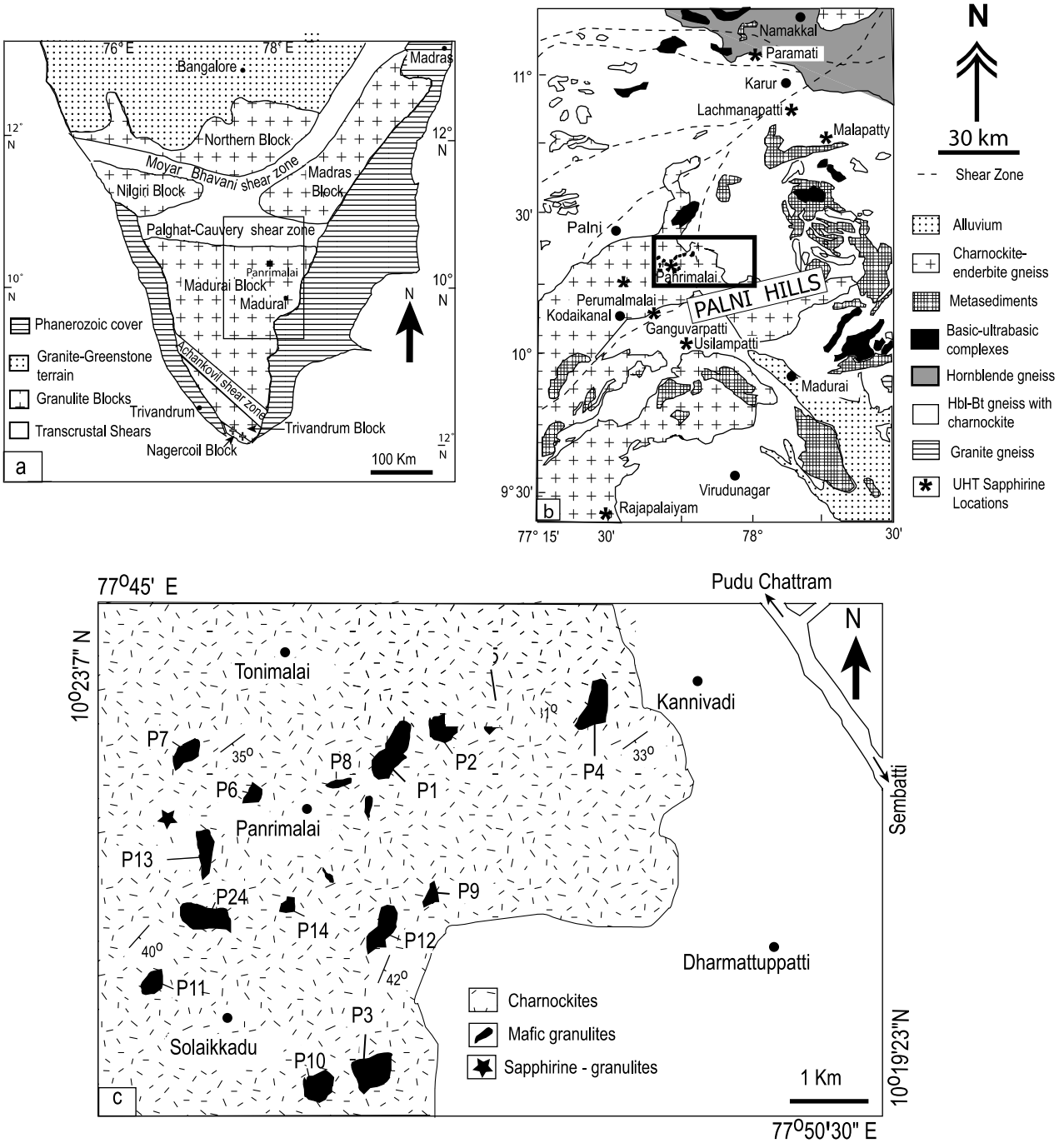


Fig. 1. (a) Map of South India showing different granulite blocks and major Proterozoic shear zones (modified from Harris et al., 1994). (b) Geological map of the Palni hills (modified from GSI, 1995). (c) Geological sketch map of the study area showing major rock types and sample locations.

between the Palghat–Cauvery and the Achankovil shear zones (Fig. 1a). The Palni hills form part of the Kodaikanal massif, one of the largest highland blocks of granulites in southern India (Fig. 1b). Charnockites, mafic granulites, metasedimentary rocks, hornblende gneiss and discrete bodies of granite comprise principal lithologies of the Palni hills. Common mineral assemblages of metapelites include garnet, cordierite, sapphirine, orthopyroxene, spinel and sillimanite. The garnet–cordierite–sapphirine-bearing assemblages dominantly occur in the central part of the highland massif while garnet–sillimanite-bearing assemblages prevail in the lowland massif such as Ganguvarpatti–Andipatti–Usilampatti. Marbles and calc-silicates constitute carbonate lithologies that locally contain quartzites and ultramafic rocks. Sapphirine-bearing granulites have been reported previously from a number of localities in the central and northern parts of the Madurai block. Many of these sapphirine granulites have registered UHT conditions (see Fig. 1b) from various localities, e.g. Rajapalaiyam (Sriramguru et al., 2002; Tateishi et al., 2004), Perumalmalai (Mohan et al., 1996; Raith et al., 1997; Prakash and Arima, 2003), Ganguvarpatti (Sajeev et al., 2004; Tamashiro et al., 2004; Mohan et al., 2005), Usilampatti (Prakash and Arima, 2003), Lachmanapatti (Tsunogae and Santosh, 2003), Malappatty (Tsunogae and Santosh, 2003), and Paramatti at the Palghat–Cauvery zone (Koshimoto et al., 2004).

The area investigated is predominantly composed of charnockites, mafic granulites and sapphirine-bearing granulites (Fig. 1c). Charnockites are common in Panrimalai and the upper Palni hill ranges. Exposures of garnet-bearing mafic granulites are scattered throughout the area. The regional strike of the foliation of the rocks in the area is dominantly NE–SW with high angle dips due SE. In their present pattern of exposure, the foliations of the mafic rocks and charnockites are parallel to the regional strike of the terrain and, hence, could be coeval. Large bands (thickness ~1–2 m) of mafic rocks occur near Solaikkadu (Fig. 2a). In places, the mafic granulites occur as smaller enclaves extending for 3–11 in. and having widths of 2–6 in. within charnockitic country rock (Fig. 2b). The rock is medium to coarse grained and dark coloured with granulitic fabric.

3. Textural relations and interpretation of metamorphic reactions

The mafic granulites of the Panrimalai area are composed mainly of orthopyroxene, clinopyroxene, and plagioclase±garnet±hornblende±biotite±quartz.

The variety of mineral associations observed in mafic granulites is summarized below:

A-I Garnet–orthopyroxene–clinopyroxene–plagioclase–hornblende–quartz, (sample nos P1, P4, P5, P9, P13).

A-II Orthopyroxene–clinopyroxene–hornblende–plagioclase–quartz (sample nos P2, P3, P8, P12, P24).

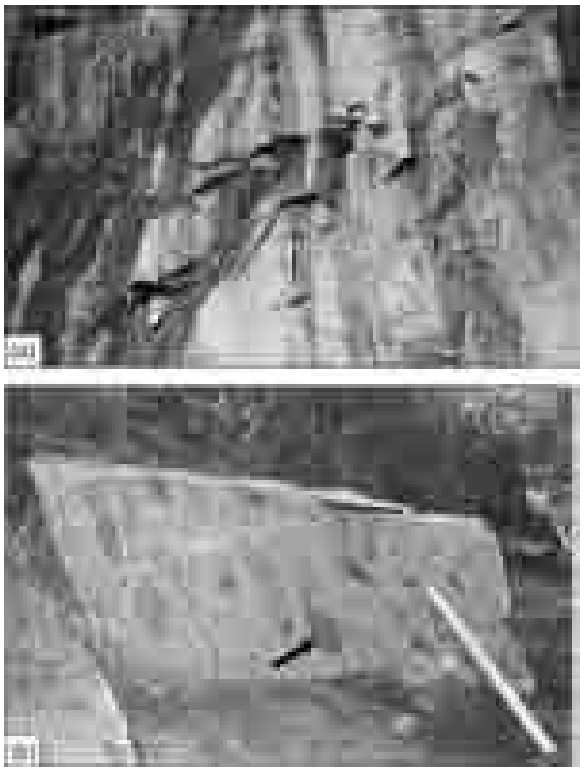


Fig. 2. (a) Field photograph showing banded (thickness of bands 1–2 m) texture in charnockite from Solaikkadu. (b) Field photograph showing mafic enclaves in charnockite at Kannivadi. These enclaves are of mafic (darker) material having 2–6 in. width and 3–11 in. length.

A-III Garnet–orthopyroxene–hornblende–plagioclase–quartz (sample nos P7, P10, P11).

A-IV Garnet–orthopyroxene–clinopyroxene–plagioclase–biotite–quartz (sample nos P6, P14).

Minor amounts of magnetite, ilmenite and apatite are also present. Mainly, two varieties of mafic granulites occur in the area, which include garnet-free and granetiferous mafic granulites. Mineral abbreviations used are taken from Kretz (1983).

Dark brown–green hornblende inclusions occur as rounded grains within orthopyroxene (Fig. 3a) and may be relicts of the prograde stage. Similar textural features reported elsewhere (Prakash, 1999a; Zhao et al., 2001) are inferred to record the prograde reaction that may have occurred during peak metamorphism:

$$Hbl_1 + qtz = opx_1 + cpx + grt + melt\ (L) \quad (1)$$

Embayed garnet porphyroblasts, engulfed in plagioclase, are separated from quartz by orthopyroxene prisms (Fig. 3b). Development of this texture is most likely the result of solid–solid vapour-absent reaction between garnet and quartz, via the following reaction:

$$Grt + qtz = opx_1 + pl_1 \quad (2)$$

Textural features and compositional plots in the Al_2O_3–($CaO + Na_2O$)–($FeO + MgO$)–SiO_2 projection (Fig. 4a) support the interpretation of reaction (2).

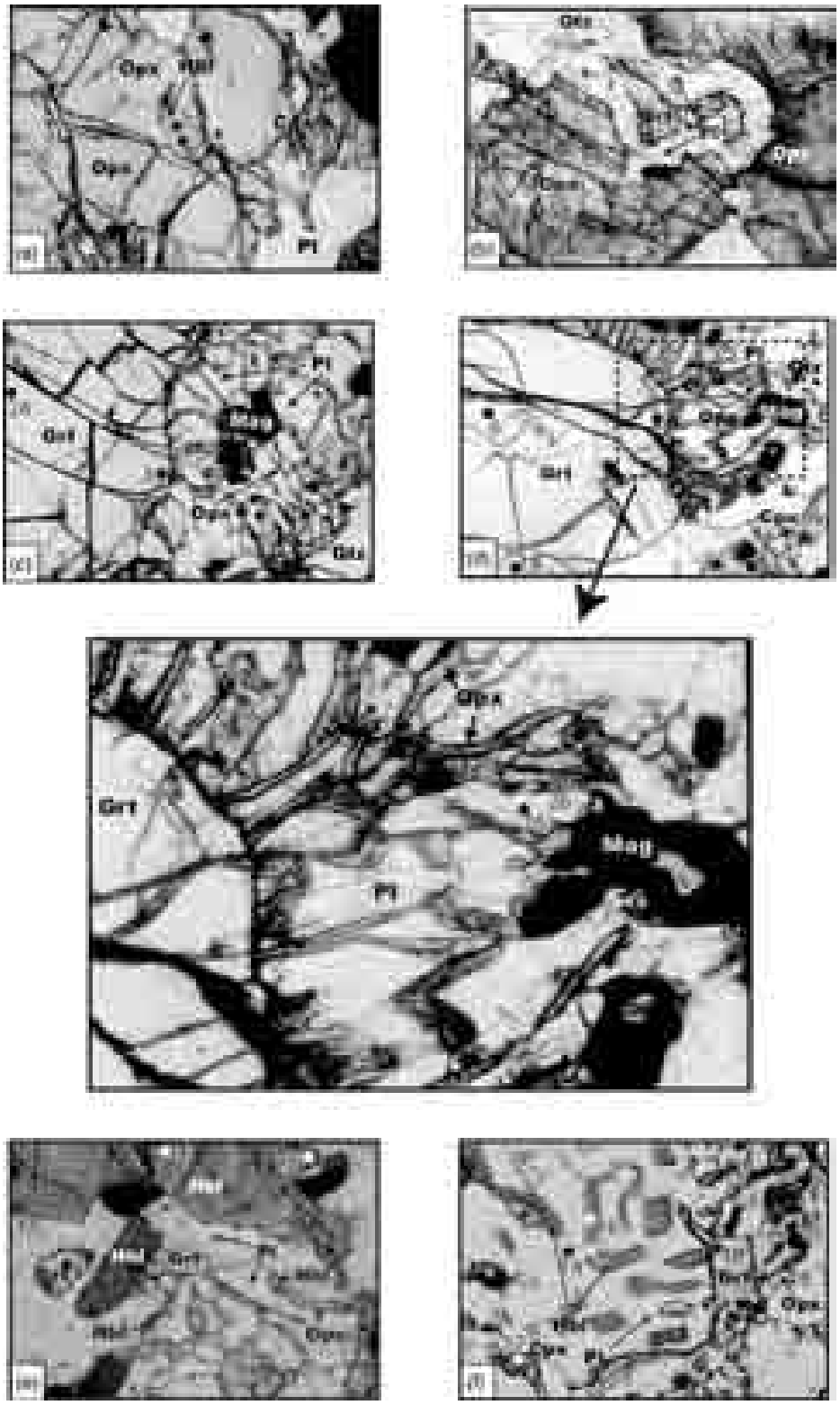


Fig. 3. Photomicrographs illustrating textural relations in the Panrimalai mafic granulites. For photographs b, c and e the width is 3 mm, whereas for photographs a, d and f the width is 1.5 mm. Locations of the analysed rim, core and symplectite mineral compositions are shown on the photomicrographs. (a) Prograde hornblende and quartz occurring as inclusions in megacrystic orthopyroxene (sample no. P12). (b) Garnet and quartz are separated by orthopyroxene and plagioclase (sample no. P6). (c) Orthopyroxene–plagioclase symplectite around embayed garnet (sample no. P1). (d) Garnet and clinopyroxene are isolated from each other by orthopyroxene–plagioclase symplectite (sample no. P4). (e) Development of orthopyroxene–plagioclase symplectite around corroded garnet–porphyroblast and hornblende (sample no. P5). (f) Hornblende–plagioclase symplectite around irregularly shaped garnet grain (sample no. P9).

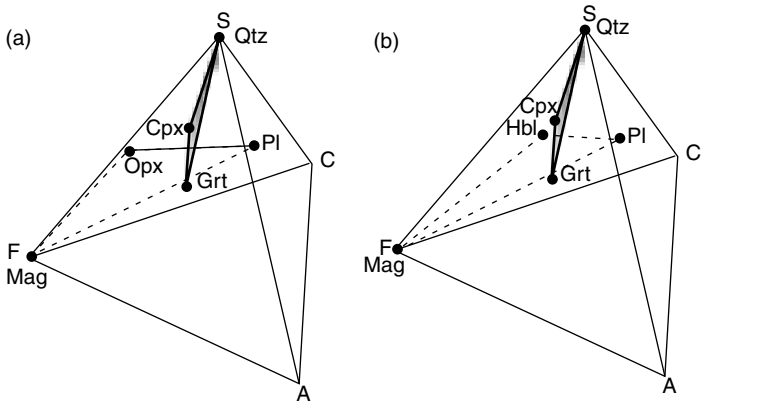


Fig. 4. Possible reactions are shown in Al_2O_3–(CaO + Na_2O)–(FeO + MgO)–SiO_2 projections for mafic granulites. Small solid circles show the plot of the analyzed mineral compositions. Mineral symbols after Kretz (1983).

Texturally, two types of orthopyroxene are present. Coarse orthopyroxene grains (up to 7 mm) are idioblastic to xenoblastic (Opx_1). The second variety of orthopyroxene (Opx_2) shows worm-like (vermicular) symplectitic intergrowths of orthopyroxene + plagioclase±magnetite (Fig. 3c–e). Embayed relicts of garnet are surrounded by spectacular radial symplectites of orthopyroxene and plagioclase without any preferred orientation (Fig. 3c–e). These textures are consistent with progress of some, or all, of the following reactions (3)–(5) (Harley, 1989; Mengel and Rivers, 1991; Thost et al., 1991; Ravindra Kumar and Chacko, 1994; Zhao et al., 2000; Ganguly et al., 2001):

$$\mathrm{Grt} + \mathrm{qtz} = \mathrm{opx}_2 + \mathrm{pl}_2 \pm \mathrm{mag} \quad (3)$$

$$\mathrm{Grt} + \mathrm{cpx} + \mathrm{qtz} = \mathrm{opx}_2 + \mathrm{pl}_2 \pm \mathrm{mag} \quad (4)$$

$$\mathrm{Grt} + \mathrm{hbl}_1 = \mathrm{opx}_2 + \mathrm{pl}_2 + \mathrm{melt\ (L)} \quad (5)$$

The fine-grained orthopyroxene–plagioclase symplectite in P4 (see enlarged Fig. 3d) mark the breakdown of garnet, according to reaction (3), which may be attributed to decompression at high T (ITD) or heating/overprinting by high T/low P. The above petrographic evidence and compositional plot of participating phases in the Al_2O_3–(CaO + Na_2O)–(FeO + MgO)–SiO_2 system (Fig. 4a) further verify reactions (3) and (4). The presence of magnetite in the above reactions suggests that ferric iron was probably present in the reacting phases. Thost et al. (1991) proposed an oxidation reaction (4), where quartz instead of being a reactant, is a product. The presence of magnetite in the orthopyroxene–plagioclase symplectites after garnet, suggests that such symplectites may result via reaction (4), promoted by oxidizing fluids. Texturally, quartz is commonly absent in symplectites or is present only in minor amounts, suggesting that a silica-bearing fluid was a reactant rather than a product phase.

Clinopyroxene is colourless to faint green in colour. Medium to coarse grained clinopyroxenes display similar textural relations as orthopyroxene (Opx_1).

Symplectites of orthopyroxene–plagioclase–hornblende occur around highly corroded garnet, clinopyroxene and quartz (Fig. 3f) that mark the following complex reaction (Ouzegane et al., 2001):

$$\mathrm{Grt} + \mathrm{cpx} + \mathrm{qtz} + \mathrm{v} = \mathrm{opx}_2 + \mathrm{pl}_2 + \mathrm{hbl}_2 \quad (6)$$

Hornblende–plagioclase symplectites around garnet porphyroblasts and clinopyroxene matrix is seen in two samples of mafic granulites. A few sections document relicts of garnet megacrysts, largely replaced by hornblende–plagioclase symplectites that may be ascribed to a garnet-consuming reaction (Mengel and Rivers, 1991; Zhao et al., 2000; Rotzler and Romer, 2001) such as:

$$\mathrm{Grt} + \mathrm{cpx} + \mathrm{qtz} + \mathrm{melt(L)} = \mathrm{pl}_2 + \mathrm{hbl}_2 \pm \mathrm{mag} \quad (7)$$

Reaction (7) is also corroborated chemographically in the Al_2O_3–(CaO + Na_2O)–(FeO + MgO)–SiO_2 projection (Fig. 4b). Zhao et al. (2001) and Norlander et al. (2002) have also reported similar textural breakdown of garnet to producing hornblende–plagioclase symplectites.

In some sections, the presence of hornblende–quartz symplectites and hornblende bordering orthopyroxene and clinopyroxene (Fig. 10a) are consistent with solid–melt back reaction, such as:

$$\mathrm{Opx} + \mathrm{cpx} + \mathrm{pl}_2 + \mathrm{melt(L)} = \mathrm{hbl}_2 + \mathrm{qtz} \quad (8)$$

Plagioclase occurs as medium to coarse-grained laths and is randomly oriented. Minute grains of plagioclase are noted in the orthopyroxene–plagioclase and hornblende–plagioclase symplectites.

It is evident from the above textural relations that the mafic granulites contained a primary assemblage of grt, opx_1, cpx, hbl_1, qtz and pl_1 that was stable during an early stage of metamorphism. The resorption of garnet through a sequence of reaction textures characterizes the subsequent symplectite stage. The presence of ubiquitous magnetite with opx_2–pl_2 symplectite indicates that some of these symplectitic textures could be ascribed to oxidation

rather than to decompression (Harley, 1989). The principal evidence favouring significant decompression comes from symplectitic pl_2 with distinctly higher anorthite—content ($An_{72–74}$) compared to matrix pl_1 ($An_{41–46}$) in the Panrimalai mafic granulites. This implies decompression as the main cause of the symplectitic texture found in the Panrimalai mafic granulites.

4. Mineral chemistry

Electron microprobe analyses were carried out on an automated energy-dispersive electron microanalyzer JEOL JSM-5300 and LINK QX2000J system, operated at an acceleration voltage of 15 kV and a specimen current of 15 nA at the Geological Institute, Yokohama National University, Japan. Analyses were refined using the LINK ZAF-4/FLS correction program. Seven representative samples were chosen for detailed analyses in order to evaluate mineral chemistry and for *P–T* calculations. The representative microprobe analyses of various minerals are listed in Tables 1a–e. Elemental maps were obtained for the elements Mg, Mn and Ca using a JEOL JCXA-8800M electron microprobe operating at 15 kV with a dwell time of 30 ms at NIPR, Tokyo. These colour coded maps are used in combination with the quantitative analytical data to demonstrate the compositional variation. The distribution of Mg, Mn and Ca in the garnet porphyroblast and orthopyroxene–plagioclase symplectite is depicted in Fig. 5a–c.

4.1. Garnet

Mafic granulites reveal that garnet is essentially almandine (54–57 mol%)–pyrope (18–24 mol%) rich. Grossular (16–18 mol%) and spessartine (4–10 mol%) components are rather low. On the basis of stoichiometric considerations, the andradite component was found to be negligible. We analyzed garnet porpyroblasts (up to 8 mm diameter) through selected compositional profiles. Generally, all garnets show minor rimward compositional zoning with narrow (< 250 μm) retrograde rims having slightly lower pyrope (av. $X_{py} = 0.23_{Core} - 0.20_{Rim}$, where $X_{Py} = Mg/Mg + Fe + Ca + Mn$). The variation in Mg within megacrystic garnet was confirmed through slight variation in colour (Fig. 5a). Spessartine component shows a minor rim-ward increase (av. $X_{sps} = 0.040_{Core} - 0.060_{Rim}$, $X_{sps} = Mn/Mg + Fe + Ca + Mn$) that was confirmed by coloured elemental maps for sample P4 (Fig. 5b). In Fig. 5b, a dark green area depicts the normal distribution of Mn in the garnet, while an enrichment of Mn was visible at narrow rims (< 350 μm) showing red and yellow colour bands. The abrupt kick-up near the rim provides evidence for the retrograde net transfer reaction (ReNTR) that can cause net growth and garnet dissolution (cf. Kohn and Spear, 2000; Prakash et al., 2006b). The most calcic plagioclase (An_{70}) occurs in symplectites, whereas the most sodic plagioclase occurs away from the garnet porphyroblast (Fig. 5c). A complete scanning profile of porphyroblastic garnet shows

Table 1a
Representative analyses of Garnet (12 oxygen basis)

Sample No.	P1	P1	P4	P4	P5	P5	P1	P4	P9	P13
Spot No.	6	13	24	2	3	7	2	3	19	14
Assemblage No.	←				A-I					→
	Core	Rim	Core	Rim	Core	Rim	Rim	Rim	Rim	Rim
	←	THERMAL PEAK STAGE			→		←	SYMPLECTITE STAGE		→
SiO_2	38.62	38.52	38.34	38.76	38.06	38.51	38.60	38.62	37.89	38.55
TiO_2	0.00	0.00	0.00	0.00	0.00	0.00	0.00	0.00	0.00	0.00
Al_2O_3	21.87	20.75	21.93	21.08	21.77	21.41	21.88	21.53	21.56	20.82
Cr_2O_3	0.26	0.00	0.00	0.00	0.00	0.00	0.00	0.00	0.00	0.44
FeO	25.38	26.73	25.56	25.17	24.43	24.74	25.32	24.76	25.01	24.42
MnO	1.95	2.71	1.69	2.58	3.08	3.07	2.92	3.42	4.34	4.07
MgO	5.27	5.07	6.09	5.78	5.85	5.51	4.73	5.56	4.66	5.02
CaO	6.38	5.92	6.14	5.92	6.01	6.60	6.01	5.95	5.96	5.97
Na_2O	0.00	0.31	0.00	0.00	0.00	0.00	0.31	0.00	0.00	0.00
K_2O	0.21	0.00	0.00	0.00	0.00	0.00	0.00	0.00	0.00	0.21
Total	99.94	100.01	99.75	99.29	99.19	99.84	99.77	99.84	99.41	99.50
Si	3.01	3.02	2.99	3.04	2.99	3.01	3.02	3.02	3.00	3.04
Ti	0.00	0.00	0.00	0.00	0.00	0.00	0.00	0.00	0.00	0.00
Al	2.01	1.92	2.01	1.95	2.01	1.97	2.02	1.98	2.01	1.93
Cr	0.02	0.00	0.00	0.00	0.00	0.00	0.00	0.00	0.00	0.03
Fe^{2+}	1.65	1.66	1.66	1.65	1.59	1.61	1.66	1.62	1.65	1.61
Fe^{3+}	0.00	0.10	0.01	0.00	0.01	0.01	0.00	0.00	0.00	0.00
Mn	0.13	0.18	0.11	0.17	0.21	0.20	0.19	0.23	0.29	0.27
Mg	0.61	0.59	0.71	0.68	0.69	0.64	0.55	0.65	0.55	0.59
Ca	0.53	0.50	0.51	0.50	0.51	0.55	0.50	0.50	0.51	0.50
Na	0.00	0.05	0.00	0.00	0.00	0.00	0.05	0.00	0.00	0.00
K	0.02	0.00	0.00	0.00	0.00	0.00	0.00	0.00	0.00	0.02
X_{Mg}	0.21	0.20	0.24	0.23	0.23	0.21	0.19	0.22	0.18	0.20

$X_{Mg} = Mg/(Mg + Ca + Mn + Fe^{2+})$, Fe^{2+} and Fe^{3+} calculated by the scheme of Droop (1987).

Table 1b
Representative analyses of Orthopyroxene (six oxygen basis)

Sample No.	P1	P1	P4	P4	P5	P5	P1	P4	P9	P13	P8	P24
Spot No.	6	9	11	13	8	7	26	34	18	14	19	21
Assemblage No.	← A-I →										← A-II →	
	Core	Rim	Core	Rim	Core	Rim	Sym	Sym	Sym	Sym	Rim	Rim
	← THERMAL PEAK STAGE →						← SYMPLECTITE STAGE →					
SiO_2	51.72	51.72	51.12	51.16	50.65	51.21	51.26	50.97	51.01	50.70	51.62	51.63
TiO_2	0.00	0.00	0.00	0.00	0.00	0.00	0.00	0.43	0.36	0.00	0.19	0.20
Al_2O_3	1.08	1.02	1.40	1.20	1.50	1.17	0.59	1.27	1.33	1.79	1.37	1.33
Cr_2O_3	0.00	0.00	0.00	0.00	0.00	0.00	0.00	0.00	0.00	0.00	0.14	0.15
FeO	28.96	29.35	27.88	27.73	27.12	27.53	29.30	27.80	27.82	27.63	28.26	28.29
MnO	0.76	0.57	1.10	1.62	1.62	1.75	0.71	1.17	1.71	1.52	0.29	0.30
MgO	16.37	15.87	16.92	16.72	16.95	17.01	16.71	16.82	16.59	16.65	17.29	17.30
CaO	0.56	0.88	0.90	0.82	1.51	0.53	0.90	0.73	0.71	0.90	0.11	0.10
Na_2O	0.36	0.46	0.33	0.36	0.00	0.00	0.00	0.00	0.39	0.00	0.00	0.00
K_2O	0.00	0.00	0.00	0.00	0.00	0.24	0.12	0.17	0.00	0.00	0.03	0.00
Total	99.80	99.86	99.65	99.60	99.33	99.44	99.60	99.34	99.93	99.20	99.30	99.30
Si	1.99	2.00	1.97	1.97	1.96	1.98	1.99	1.97	1.97	1.97	1.99	1.99
Ti	0.00	0.00	0.00	0.00	0.00	0.00	0.00	0.01	0.01	0.00	0.01	0.01
Al	0.05	0.05	0.06	0.05	0.07	0.05	0.03	0.06	0.06	0.08	0.06	0.06
Cr	0.00	0.00	0.00	0.00	0.00	0.00	0.00	0.00	0.00	0.00	0.00	0.00
Fe^{2+}	0.93	0.95	0.87	0.87	0.87	0.89	0.95	0.90	0.88	0.90	0.91	0.91
Fe^{3+}	0.00	0.00	0.02	0.02	0.01	0.00	0.00	0.00	0.02	0.00	0.00	0.00
Mn	0.02	0.02	0.04	0.05	0.05	0.06	0.02	0.04	0.06	0.05	0.01	0.01
Mg	0.94	0.91	0.97	0.96	0.98	0.98	0.97	0.97	0.95	0.96	0.99	0.99
Ca	0.02	0.04	0.04	0.03	0.06	0.02	0.04	0.03	0.03	0.04	0.00	0.00
Na	0.03	0.03	0.02	0.03	0.00	0.00	0.00	0.00	0.03	0.00	0.00	0.00
K	0.00	0.00	0.00	0.00	0.00	0.01	0.01	0.01	0.00	0.00	0.00	0.00
X_{Mg}	0.50	0.49	0.53	0.52	0.53	0.52	0.50	0.51	0.52	0.52	0.52	0.52

$X_{Mg} = Mg/(Mg + Ca + Mn + Fe^{2+})$, Fe^{2+} and Fe^{3+} calculated by the scheme of Droop (1987).

Table 1c
Representative analyses of Plagioclase (eight oxygen basis)

Sample No.	P1	P1	P4	P4	P5	P5	P1	P4	P9	P13	P8	P24
Spot No.	32	36	7	11	19	21	16	21	14	34	21	6
Assemblage No.	← A-I →										← A-II →	
	Core	Rim	Core	Rim	Core	Rim	Sym	Sym	Sym	Sym	Rim	Rim
	← THERMAL PEAK STAGE →						← SYMPLECTITE STAGE →					
SiO_2	57.24	56.96	58.07	56.32	56.62	57.01	49.25	48.81	48.50	49.45	48.57	48.54
TiO_2	0.00	0.27	0.00	0.00	0.36	0.00	0.00	0.00	0.00	0.00	0.00	0.00
Al_2O_3	26.82	27.08	25.79	27.44	27.27	26.98	32.28	32.91	33.21	32.40	33.11	33.22
Cr_2O_3	0.00	0.00	0.31	0.00	0.00	0.00	0.00	0.00	0.00	0.00	0.00	0.00
FeO	0.00	0.51	0.00	0.00	0.00	0.00	0.31	0.00	0.00	0.00	0.00	0.00
MnO	0.36	0.00	0.00	0.00	0.00	0.00	0.00	0.00	0.00	0.00	0.00	0.00
MgO	0.00	0.00	0.00	0.00	0.00	0.00	0.00	0.00	0.00	0.00	0.00	0.00
CaO	8.63	8.38	8.52	9.46	8.65	8.69	14.96	14.66	14.59	14.53	14.60	14.63
Na_2O	6.25	6.21	6.31	5.74	6.11	6.37	2.87	3.06	2.86	2.88	2.87	2.88
K_2O	0.47	0.53	0.63	0.76	0.44	0.46	0.12	0.00	0.00	0.26	0.00	0.00
Total	99.77	99.95	99.61	99.71	99.45	99.51	99.79	99.44	99.15	99.51	99.15	99.27
Si	2.58	2.56	2.61	2.54	2.55	2.57	2.26	2.24	2.23	2.26	2.23	2.23
Ti	0.00	0.01	0.00	0.00	0.01	0.00	0.00	0.00	0.00	0.00	0.00	0.00
Al	1.42	1.43	1.37	1.46	1.45	1.43	1.74	1.78	1.80	1.75	1.79	1.80
Cr	0.00	0.00	0.01	0.00	0.00	0.00	0.00	0.00	0.00	0.00	0.00	0.00
Fe	0.00	0.02	0.00	0.00	0.00	0.00	0.01	0.00	0.00	0.00	0.00	0.00
Mn	0.01	0.00	0.00	0.00	0.00	0.00	0.00	0.00	0.00	0.00	0.00	0.00
Mg	0.00	0.00	0.00	0.00	0.00	0.00	0.00	0.00	0.00	0.00	0.00	0.00
Ca	0.42	0.40	0.41	0.46	0.42	0.42	0.73	0.72	0.72	0.71	0.72	0.72
Na	0.54	0.54	0.55	0.50	0.53	0.56	0.25	0.27	0.25	0.26	0.26	0.26
K	0.03	0.03	0.04	0.04	0.03	0.03	0.01	0.00	0.00	0.02	0.00	0.00
X_{An}	0.42	0.41	0.41	0.46	0.43	0.42	0.74	0.73	0.74	0.72	0.74	0.74

Table 1d
Representative analyses of Clinopyroxene (six oxygen basis)

Sample No.	P1	P1	P4	P4	P5	P5	P1	P4	P9	P13	P8	P24
Spot No.	13	7	17	19	23	26	11	23	17	24	6	11
Assemblage No.	←				A-I					→	← A-II	→
	Core	Rim	Core	Rim	Core	Rim	Rim	Rim	Rim	Rim	Rim	Rim
	← THERMAL PEAK STAGE →						← SYMPLECTITE STAGE →					
SiO_2	52.14	52.06	51.78	51.63	51.03	51.38	52.52	52.15	51.48	51.66	52.50	52.49
TiO_2	0.00	0.00	0.39	0.55	0.71	0.45	0.00	0.29	0.00	0.00	0.00	0.00
Al_2O_3	1.88	2.11	1.89	2.57	2.71	2.54	2.24	2.89	2.56	2.54	2.21	2.22
Cr_2O_3	0.00	0.00	0.00	0.00	0.00	0.00	0.00	0.00	0.00	0.00	0.00	0.00
FeO	13.11	13.63	12.40	12.44	11.81	12.16	12.88	12.55	11.87	11.83	12.86	12.90
MnO	0.00	0.00	0.41	0.00	0.74	0.84	0.33	0.84	0.71	0.83	0.32	0.32
MgO	11.46	11.05	11.51	11.74	11.32	11.49	12.24	12.72	11.73	11.70	12.21	12.23
CaO	19.99	19.81	20.84	19.27	21.06	20.17	18.85	17.74	20.75	20.14	18.87	18.90
Na_2O	0.69	0.59	0.57	0.86	0.43	0.54	0.69	0.75	0.67	0.65	0.67	0.63
K_2O	0.00	0.00	0.00	0.00	0.00	0.00	0.00	0.00	0.00	0.00	0.00	0.00
Total	99.27	99.25	99.79	99.07	99.81	99.56	99.75	99.93	99.76	99.33	99.64	99.69
Si	1.98	1.98	1.96	1.96	1.93	1.95	1.98	1.96	1.94	1.96	1.98	1.98
Ti	0.00	0.00	0.01	0.02	0.02	0.01	0.00	0.01	0.00	0.00	0.00	0.00
Al	0.08	0.09	0.08	0.12	0.12	0.11	0.10	0.13	0.11	0.11	0.10	0.10
Cr	0.00	0.00	0.00	0.00	0.00	0.00	0.00	0.00	0.00	0.00	0.00	0.00
Fe^{2+}	0.42	0.43	0.38	0.40	0.37	0.39	0.41	0.39	0.32	0.36	0.41	0.41
Fe^{3+}	0.00	0.00	0.01	0.00	0.00	0.00	0.00	0.00	0.05	0.02	0.00	0.00
Mn	0.00	0.00	0.01	0.00	0.02	0.03	0.01	0.03	0.02	0.03	0.01	0.01
Mg	0.65	0.63	0.65	0.66	0.64	0.65	0.69	0.71	0.66	0.66	0.69	0.69
Ca	0.81	0.81	0.85	0.78	0.86	0.82	0.76	0.71	0.84	0.82	0.76	0.76
Na	0.05	0.04	0.04	0.06	0.03	0.04	0.05	0.05	0.05	0.05	0.05	0.05
K	0.00	0.00	0.00	0.00	0.00	0.00	0.00	0.00	0.00	0.00	0.00	0.00
X_{Mg}	0.61	0.59	0.63	0.62	0.63	0.63	0.63	0.64	0..67	0.65	0.63	0.63

$X_{Mg} = Mg/(Mg + Fe^{2+})$, Fe^{2+} and Fe^{3+} calculated by the scheme of Droop (1987).

Table 1e
Representative analyses of Hornblende (23 oxygen basis)

Sample No.	P12	P12	P1	P1	P4	P4	P5	P5	P9	P13	P8	P24
Spot No.	7	8	8	13	16	23	17	21	16	8	11	27
Assemblage No.	← A-II →		←			A-I				→	← A-II	→
	CORE	CORE	Core	Rim	Core	Rim	Core	Rim	Sym	Sym	Sym	Sym
	PROGRADE STAGE		←	→	THERMAL PEAK STAGE		→		← SYMPLECTITE STAGE		→	
SiO_2	41.83	42.27	43.06	42.96	43.65	42.62	42.25	42.41	41.40	40.35	41.74	41.75
TiO_2	3.07	3.24	2.95	2.64	2.28	2.35	2.82	2.51	0.77	1.88	0.84	0.86
Al_2O_3	12.10	11.81	12.44	12.40	13.43	12.74	12.59	13.12	13.56	13.42	13.44	13.46
Cr_2O_3	0.00	0.00	0.00	0.00	0.00	0.00	0.00	0.00	0.00	0.00	0.33	0.36
FeO	19.18	18.13	15.45	17.02	14.95	17.47	16.70	16.78	18.81	18.00	17.75	17.79
MnO	0.00	0.83	0.00	0.00	0.00	0.00	0.00	0.00	0.00	0.63	0.00	0.00
MgO	8.49	8.70	9.26	9.10	9.47	8.56	9.69	9.49	10.00	9.59	9.51	9.52
CaO	10.56	10.91	10.63	10.99	9.94	11.04	11.14	11.07	10.68	10.90	11.53	11.50
Na_2O	1.34	1.47	3.07	1.99	2.61	1.97	1.85	1.99	1.86	1.67	1.56	1.56
K_2O	1.92	1.64	1.69	1.97	1.62	1.91	1.81	1.58	1.73	2.31	1.85	1.85
Total	98.48	98.99	98.54	99.06	97.95	98.65	98.84	98.95	98.80	98.76	98.55	98.65
Si	6.24	6.28	6.40	6.39	6.46	6.38	6.27	6.27	6.07	6.00	6.20	6.20
Ti	0.34	0.36	0.33	0.30	0.25	0.26	0.31	0.28	0.08	0.21	0.09	0.10
Al	2.13	2.07	2.18	2.18	2.34	2.25	2.20	2.29	2.35	2.35	2.35	2.35
Cr	0.00	0.00	0.00	0.00	0.00	0.00	0.00	0.00	0.00	0.00	0.04	0.04
Fe^{2+}	1.83	1.82	1.92	2.12	1.84	2.19	1.86	1.83	1.18	1.39	1.66	1.64
Fe^{3+}	0.56	0.43	0.00	0.00	0.02	0.00	0.22	0.24	1.12	0.84	0.56	0.57
Mn	0.00	0.10	0.00	0.00	0.00	0.00	0.00	0.00	0.00	0.08	0.00	0.00
Mg	1.89	1.93	2.05	2.02	2.09	1.91	2.14	2.09	2.19	2.12	2.11	2.11
Ca	1.69	1.74	1.69	1.75	1.58	1.77	1.77	1.75	1.68	1.74	1.84	1.83
Na	0.39	0.42	0.88	0.57	0.75	0.57	0.53	0.57	0.53	0.48	0.45	0.45
K	0.37	0.31	0.32	0.37	0.31	0.37	0.34	0.30	0.32	0.44	0.35	0.35
Name	Tschermakite		Pargasite	Ferro-Pargasite	Pargasite	Ferro-Pargasite	Pargasite	Pargasite	Magnesio-Hastingsite	Magnesio-Hastingsite	Magnesio-Hastingsite	Magnesio-Hastingsite

Fe^{2+} and Fe^{3+} calculated by the scheme of Droop (1987).

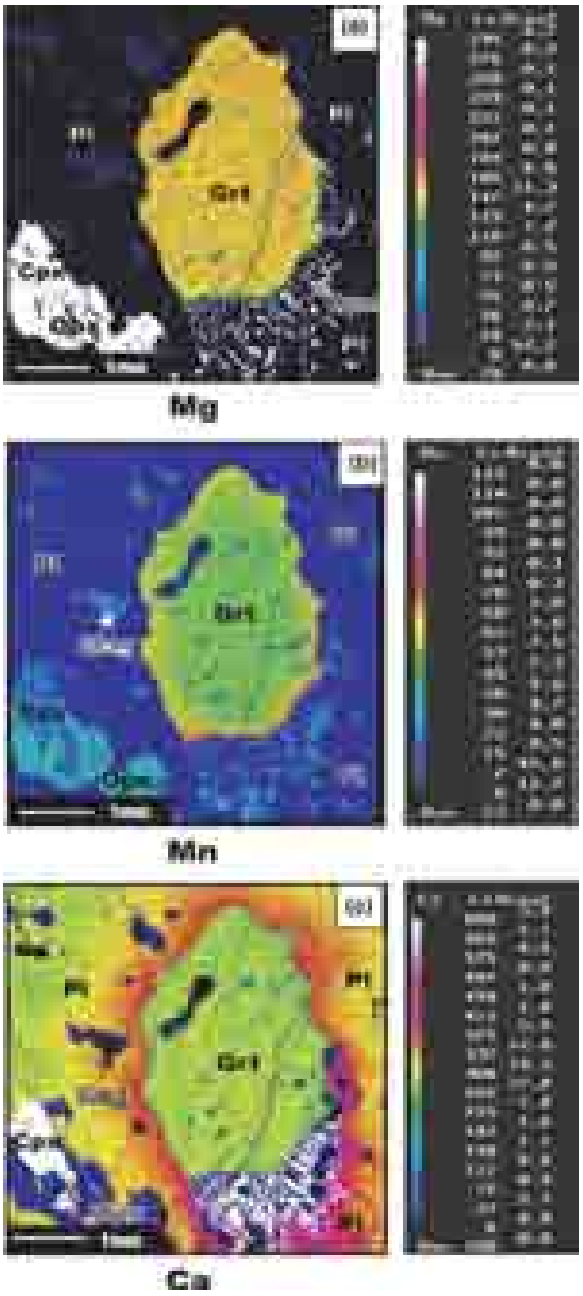


Fig. 5. Colour-coded compositional maps showing the element distribution in the garnet porpyroblast and orthopyroxene–plagioclase symplectites. (a)–(c) Display the distribution of Mg, Mn and Ca, respectively (sample no. P4).

minor decrease in grossular component from core to rim located close to the orthopyroxene–plagioclase intergrowth (av. $X_{Grs} = 0.18_{Core} - 0.17_{Rim}$, where $X_{Grs} = Ca/Mg + Fe + Ca + Mn$; Fig. 5c).

4.2. Pyroxene

Orthopyroxene forms a solid-solution between enstatite and ferrosilite with a maximum X_{Mg} of 0.53 (where $X_{Mg} = Mg/(Mg + Fe^{2+})$). The Al and Fe^{3+} contents of orthopyroxene are usually low. The highest Al_2O_3 content reaches 1.79 wt%. The low values makes it difficult to apply Al-in-Opx thermobarometery with precision, and also renders retrival calculations to be model-dependent. Prismatic orthopyroxenes do not show distinct compositional zoning. No significant difference in composition between matrix and the symplectitic orthopyroxene is noted. The plot of orthopyroxene composition lies close to the hypersthene ($En_{48–56}$) composition while the coexisting clinopyroxenes occupy the diopside–augite field. X_{Mg} of clinopyroxene ranges from 0.59 to 0.67.

4.3. Plagioclase

Plagioclase shows compositional variation with respect to An-content. The matrix plagioclase is andesine ($An_{41–46}$) for both rim and core composition. Plagioclase with the orthopyroxene/hornblende±magnetite symplectites is more calcic ($An_{72–74}$) than the matrix plagioclase, which is further confirmed by coloured elemental maps (Fig. 5c). The red to yellow coloured areas depict lower Ca—content in the plagioclase, while enrichment of Ca is visible in regions showing white.

4.4. Hornblende

Hornblende analyses have been normalized to the 13ex CNK scheme of Robinson et al. (1982) and the nomenclature used follows (Leake et al. 1997). The Fe^{3+}-content calculated from Droop (1987) Eq. no. (6) gives a maximum Fe^{3+} estimate and reaches 1.123. The X_{Mg} values after Fe^{3+} extraction range from 0.47 to 0.65. Typically, the brown prograde hornblende is Tschermakite containing a higher amount of TiO_2. The matrix compositions of the hornblende are pargasite to ferro-pargasite; whereas, the symplectite compositions are magnesio-hastingsite. Their molecular Si-content is different for the matrix hornblende (av. 6.36) and the symplectite hornblende (av. 6.11). Compared to matrix hornblende, higher FeO and Al_2O_3 and significantly lower TiO_2 are noted in the symplectitic hornblende. The TiO_2 content of the prograde hornblende is relatively high (~3.0 wt%) in contrast to the Ti content of later hornblende (commonly > 2 wt% for matrix and < 2 wt% for symplectite). Hornblende grains in contact with ilmenite contain less Ti than those associated with orthopyroxene, clinopyroxene and plagioclase. These variations in Ti-content are also dependent on the Fe–Mg ratio of the hornblende.

5. Petrogenetic grid

A petrogenetic grid for the mafic granulites in the model system CaO–(FeO + MgO)–Al_2O_3 + SiO_2–H_2O (CMASH), modified after Pattison (2003) is depicted in Fig. 10a. The topology of the divariant fields is shown in the ACF diagram. Considering quartz and melt as excess phases, the system CaO–(FeO + MgO)–Al_2O_3–SiO_2–H_2O reduces to a three component system Al_2O_3–CaO–(FeO + MgO).

The P–T slopes of the reactions in Fig. 10a are schematic but consistent with that of experiments and thermodynamic modeling (Pattison, 2003). Arrow shows the P–T path for the prograde and retrograde reactions deduced from the textural and the phase compatibility relations.

6. Geothermobarometric calculations

The P–T evolution of the garnet-bearing mafic granulites has been constrained through the use of conventional thermobarometry as well as the internally consistent TWQ program (versions 2.02 and 1.02; Berman, 1991; updated 1997). For a characterization of the P–T regime during metamorphism, the garnetiferous lithologies are most suitable, since a set of reasonably well-calibrated geothermobarometers based on Fe–Mg exchange equilibria and pressure-sensitive net-transfer reactions are available. Mineral thermobarometry may give unreliable P–T because of post-peak diffusional and closure effects (Frost and Chacko, 1989; Harley, 1998). Where quartz is not present, the temperatures indicate a maximum, and the pressures a minimum. In the TWQ program, P and T were determined from the intersection of three or more independent reactions in P–T space, using the thermodynamic datasets of Berman (1988), Berman et al. (1995) and Berman and Aranovich (1996) for end-member phases. The different mineral equilibria have been calculated using ideal solution models for orthopyroxene and clinopyroxene (Newton, 1983) and the solution models of Berman (1990), Fuhrman and Lindsley (1988) and Madar et al. (1994) for garnet, plagioclase and amphibole, respectively. For precision, only those P–T values from the equilibria intersection which yield $\sigma < \pm 0.5$ kbar and ± 20 °C were considered.

6.1. Prograde stage

In a few cases, relict brown hornblende inclusions occur as rounded grains within the coarse prisms of orthopyroxene (Fig. 3a). The brown Tschermakitic hornblende with distinctly higher TiO_2 content is interpreted as part of the primary paragenesis. It is difficult to quantitavely estimate P–T conditions for the prograde stage. However, the presence of sillimanite pseudomorph after kyanite blades (Palni: Raith et al., 1997), coexistence of kyanite + staurolite (Kiranur: Lal et al., 1984) and oval gedrite inclusions within coarse orthopyroxene prisms (Ganguvarpatti: Mohan and Lal, 1986) recorded from the adjoining areas within the Madurai block lend support for the prograde CW limb passing through kyanite and sillimanite equilibrium. The textural evidence from adjacent areas and from the present study help in interpreting the onset of the plagioclase-absent reaction (1) within the kyanite stability field (Fig. 10a).

6.2. Thermal peak stage

The end-member phases used in the TWQ calculation were pyrope, almandine, ferrosilite, orthoenstatite, hedenbergite, diopside, anorthite and beta-quartz. Among the 11 possible equilibria that can be written for the selected end-member phases, only three are linearly independent (Table 2). Core compositions for samples P1, P4 and P5 give a precise intersection using these equilibria (Fig. 6), suggesting near-thermal peak conditions of granulite-facies metamorphism > 900 °C at 9 kbar. The pressure values 8.5–9.5 kbar at the thermal maxima give an upper limit, but the actual peak pressures may be lowered by 1 kbar. The P–T conditions calculated using the TWQ program (version 2.02) compare well with those obtained from conventional thermobarometry (Table 3) and feldspar thermometery. We have used the Fe–Mg garnet–orthopyroxene thermometer of Harley (1984); calculated temperatures for the core and the rim compositions for mafic granulites are 800±10 and 790±20 °C, respectively. Harley's calibration (1984) gives 100–200 °C lower T estimates, unlike the peak metamorphic temperatures (Harley, 1998). The thermometric models of Sen and Bhattacharya (1984), Aranovich and Podlesskii (1989) and Lal (1993) provide average temperatures of 900±20 and 890±30 °C for core and rim, respectively. However, the temperature values are raised by a minimum of 50–100 °C using the model of Lee and Ganguly (1988). The estimated temperatures using the calibrations of Ellis and Green (1979) and Pattison and Newton (1989) are 842±16 °C (core) and 840±15 °C (rim).

Table 2
Simultaneous calculation of P–T by TWQ program (version 2.02)

	Equilibria plotted in Figs. 6 and 7	ΔS (J K^{-1})	ΔV (J bar^{-1})
1.	Qtz + Hd + Alm = An + 4 Fsl	−24.6	−2.57
2.	Qtz + Di + Alm = An + 3 Fsl + En	−28.1	−2.59
3.	3 Qtz + 3 Di + 4 Alm = 3An + 12 Fsl + Prp	−103.5	−8.04
4.	En + Hd = Di + Fsl	3.5	0.02
5.	Alm + 4 Di + Qtz = 4 En + 3 Hd + An	−38.7	−2.66
6.	Alm + 3 Di = Prp + 3 Hd	−29.6	0.34
7.	Qtz + Prp + 4 Hd = An + 3 Di + 4 Fsl	5.0	−2.23
8.	Alm + 3 En = Prp + 3 Fsl	−19.1	−0.27
9.	Qtz + Prp + Di = An + 4 En	−9.1	−2.32
10.	3 Qtz + 4 Prp + 3 Hd = Alm + 3 An + 12 En	2.4	−6.62
11.	Qtz + Prp + Hd = An + Fsl + 3 En	−5.6	−2.30

Phases used in calculation: Alm, almandine; Prp, pyrope; Fsl, ferrosilite; En, orthoenstatite; Hd, hedenbergite; Di, diopside; An, anorthite; Qtz, beta-quartz. ΔS and ΔV are calculated at 1 bar and 298 K.

Pressure estimates were obtained from garnet–orthopyroxene–plagioclase–quartz assemblages employing five different calibrations (Table 3). These yielded differences of 0.3–0.8 kbar in pressure values for P_{Mg} and P_{Fe}, respectively. Such variation in absolute pressure values could be related to the uncertainties associated with thermochemical data in locating the end-member reactions. Our pressure estimates for mafic granulites (calculated at 900 °C) range from 8.4 to 10 kbar with most pressure values falling between 8.8 and 9.6 kbar. These independent pressure estimates overlap with the results obtained from the TWQ program.

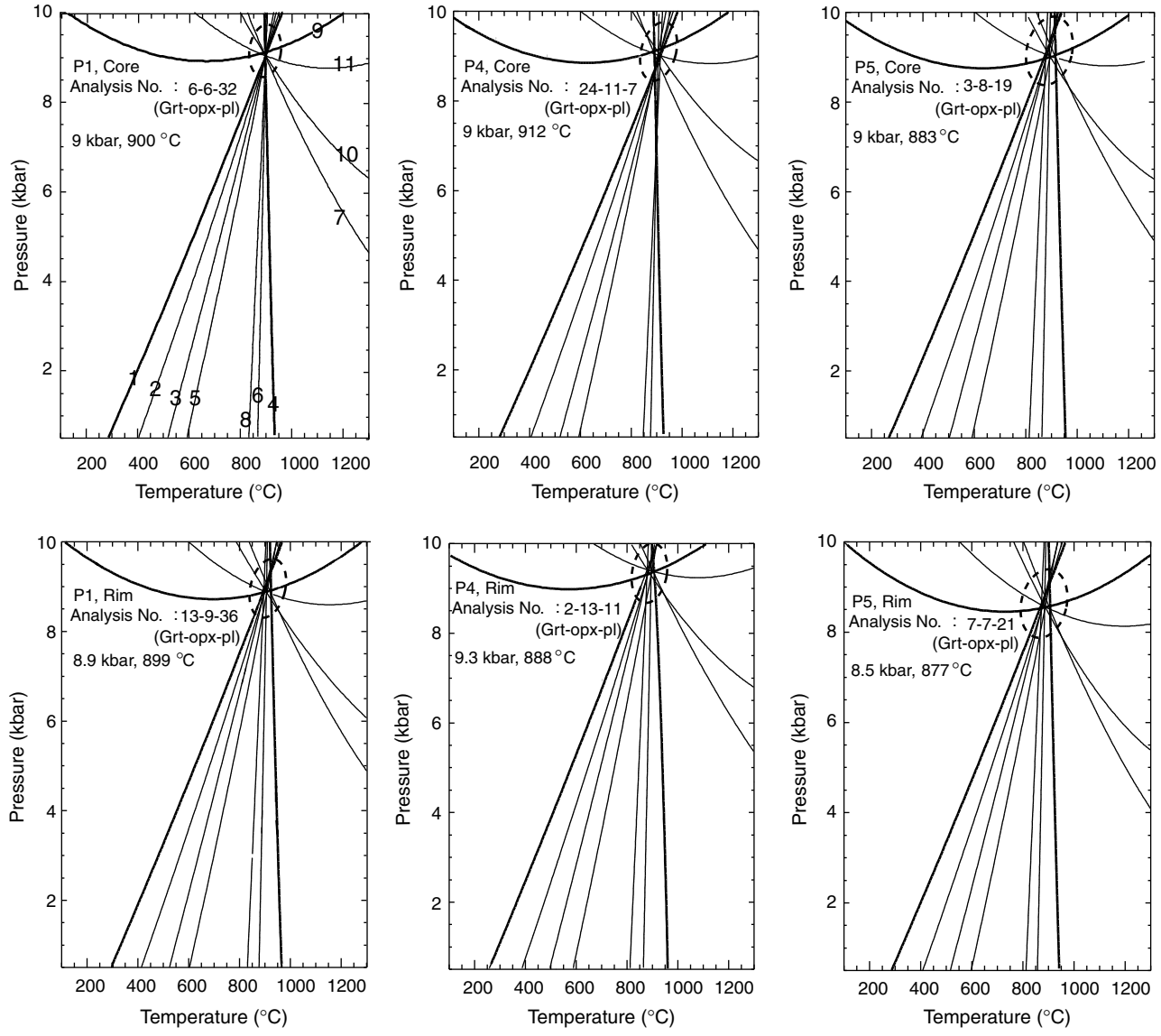


Fig. 6. TWQ (version 2.02) results for close-to-peak metamorphic stage. The specific equilibria are listed in Table 2. Errors are shown by dotted ellipses. The bold lines show independent reactions.

The garnet–clinopyroxene–plagioclase–quartz assemblage permits the use of the calibrations of Moecher et al. (1988) and Eckert et al. (1991) to estimate pressure conditions of chemical equilibration. The calculated pressures from the model of Moecher et al. (1988) yield higher values by 0.4–0.6 kbar compared to the calibration of Eckert et al. (1991), probably representing an overestimation (see Table 3). Variations in pressure estimates are a consequence of the difference in the activity-composition relations and the thermodynamic data utilized in these models.

The different closure temperatures in exchange thermometers and net-transfer reactions have limitations on the reliability of conventional thermobarometery to calculate the thermal peak of HT/UHT rocks. The reasonable convergence from the above thermobarometers would be > 900 °C at ≤ 9 kbar.

6.3. Symplectite stage

P–T calculations for symplectite assemblages were attempted on re-equilibrated garnet rims adjacent to orthopyroxene–hornblende–plagioclase symplectites. End-member phases and their solid solution models used for the early stage assemblage were also selected for these symplectites, and 11 possible equilibria for the end-member phases (three independent) are shown in Table 2. Using these equilibria, garnet rims and orthopyroxene–plagioclase symplectite compositions for samples P1, P4, P9, P13 give a precise intersection at ca. 6.5 kbar at 820 °C, thus lending support for a decompressional path (Fig. 7).

We also used the garnet–orthopyroxene–plagioclase–quartz barometer for estimating pressure conditions of orthopyroxene–plagioclase symplectites. Calibrations of

Table 3
P–T results using preferred models of geothermobarometery

	P1, Core	P1, Rim	P4, Core	P4, Rim	P5, Core	P5, Rim	P1, Sym	P4, Sym	P9, Sym	P13, Sym
Thermometry (°C)										
Grt–Opx										
Sen and Bhattacharya (1984)	902	904	937	931	921	870	797	877	754	820
Harley (1984)	790	791	816	812	806	769	713	772	682	731
Lee and Ganguly (1988)	959	970	980	976	992	951	885	959	868	923
Aranovich and Podlesskii (1989)	903	903	919	913	901	876	838	876	792	832
Lal (1993)	856	854	875	870	858	830	785	827	746	786
Grt–Cpx										
Ellis and Green (1979)	832	835	843	845	842	832	756	786	700	755
Ganguly (1979)	910	925	928	924	936	918	852	886	811	862
Pattison and Newton (1989)	834	864	850	859	850	824	720	769	634	719
Barometry (kbar)										
Grt–Opx–Pl—Qtz										
Bohlen et al. (1983)	9.3	9.0	9.4	9.7	9.3	9.4	4.1	4.1	4.2	4.1
Perkins and Chipera (1985), P_{Mg}	10.2	9.8	10.3	10.5	9.8	9.7	6.4	6.7	6.0	6.4
Perkins and Chipera (1985), P_{Fe}	9.7	9.3	9.8	10.1	9.7	9.8	5.2	5.2	5.4	5.2
Eckert et al. (1991)	9.5	9.2	9.9	10.2	9.6	9.2	6.2	6.8	5.9	6.4
Bhattacharya et al. (1991), P_{Mg}	9.3	8.8	9.3	9.6	9.0	8.9	6.3	6.7	5.7	6.2
Bhattacharya et al. (1991), P_{Fe}	8.6	8.2	8.4	8.7	8.2	8.5	4.5	4.3	4.4	4.3
Lal (1993), P_{Mg}	8.8	8.4	8.9	9.3	8.6	8.4	7.2	7.4	6.6	7.0
Lal (1993), P_{Fe}	9.4	9.1	9.2	9.6	9.2	9.4	4.4	4.5	4.4	4.4
Grt–Cpx–Pl–Qtz										
Moecher et al. (1988), P_{Mg}	10.3	9.9	10.2	10.4	9.7	10.5	7.0	7.3	6.1	6.5
Moecher et al. (1988), P_{Fe}	10.3	9.6	10.1	10.2	9.7	10.5	5.2	5.3	5.0	4.9
Eckert et al. (1991)	9.8	9.3	9.8	9.9	9.3	9.9	6.7	7.2	5.9	6.4
Grt–Hbl–Pl—Qtz										
Kohn and Spear (1989), P_{Mg}	8.6	8.4	8.5	8.3	8.7	9.0	–	–	5.2	5.9
Kohn and Spear (1989), P_{Fe}	9.2	8.8	9.0	8.2	9.1	9.5	–	–	7.0	7.0

Core and rim *P–T* estimates calculated at 9 kbar and 900 °C. *P–T* estimates from symplectitic assemblages calculated at 6 kbar and 800 °C.

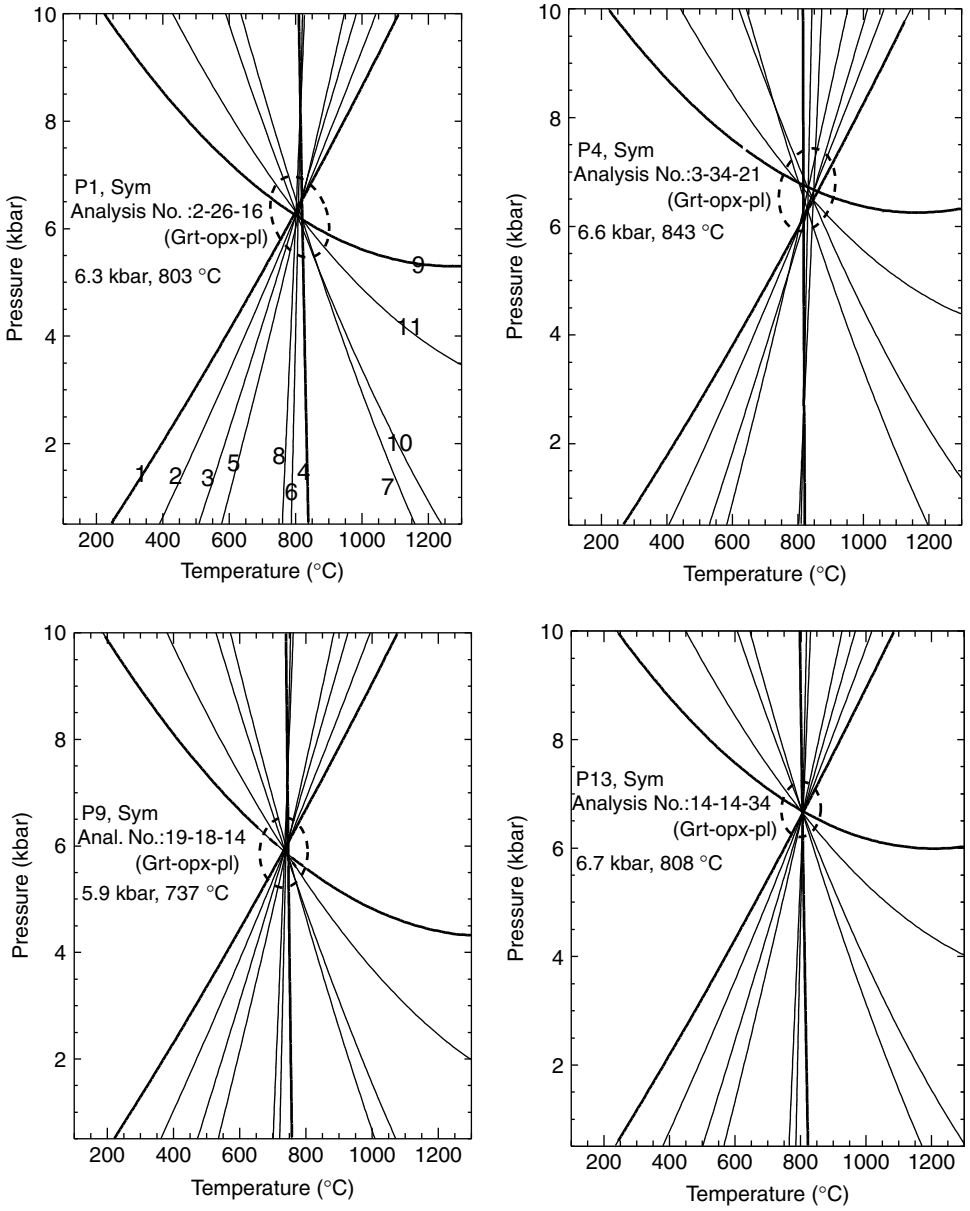


Fig. 7. TWQ (version 2.02) results for orthopyroxene–plagioclase symplectitic stage. The specific equilibria are listed in Table 2.

Eckert et al. (1991), Bhattacharya et al. (1991) and Lal (1993) yield broadly similar results (ca. 6.5 kbar), which are in close agreement with P estimates obtained from the TWQ program. Other calibrations (see Table 3) that provide a wide P–T range for the symplectitic assemblage possibly relate to errors inherited in the calibrations, and to a certain extent, late re-equilibration as well.

Similarly for the hornblende–plagioclase symplectites, the phases involved in the TWQ calculation include almandine, pyrope, grossular, pargasite, ferro-pargasite, tschermakite, albite (low), anorthite, and beta-quartz. The TWQ results based on the intersection of four possible equilibria for samples P9 and P13 are given in Table 4 and shown in Fig. 8. The lower P–T conditions at ca. 5.5 kbar/780 °C resulted in the breakdown of highly corroded garnet and development of hornblende–plagioclase symplectites during decompression. For late stage hornblende–quartz symplectites (Fig. 8c and d), the equilibria involved in the calculation include ferrosilite, orthoenstatite, hedenbergite, diopside, pargasite, beta-quartz, and water (P8 and P24). The water activities were calculated at the anhydrous multi-equilibrium pressure results derived above and the activity of water obtained is 0.25. Samples P8 and P24 yielded lower PT results for the hornblende–quartz symplectites that fall in the range of 4.3 kbar/740 °C to 4.5 kbar/743 °C.

7. Feldspar thermometry

Recently, Yoshimura et al. (2000) and Hokada (2001), and Prakash et al. (2006a) and others showed that the

Table 4
Simultaneous calculation of P–T by TWQ program (version 1.02)

	ΔS (J K^{-1})	ΔV (J bar^{-1})
Equilibria plotted in Fig. 8a and b[a]		
1. 3 Ab + 2 Grs + Prp + 3 Tsc = 3 Parg + 6 Qtz + 6 An	−279.0	−8.66
2. 12 Tsc + 8 Grs + 4 Alm + 12 Ab = 24 An + 24 Qtz + 9 Parg + 3 FePa	−1271.1	−36.18
3. 3 Parg + 4 Alm = 4 Prp + 3 FePa	− 155.1	−1.52
4. 3 Ab + 4 Alm + 2 Grs + 3 Tsc = 3 FePa + 6 Qtz + 3 Prp + 6 An	− 434.1	−10.19
Equilibria plotted in Fig. 8c and d[b]		
1. 2 Di + Fsl = 2 Hd + En	4.24	0.02
2. 2 Ab + 2 An + 2 Di + 3 En + 2 W = 2 Parg + 8 Qtz	0.84	0.79
3. 2Ab + 2 An + 4 En + 2 Hd + 2 W = 2 Parg + 8 Qtz + Fsl	− 3.40	0.76
4. 2 Ab + 2 An + 8 Di + 3 Fsl + 2 W = 2 Parg + 8 Qtz + 6 Hd	13.55	0.86

ΔS and ΔV are calculated at 1 bar and 298 K.
[a] Phases used in calculation: Alm, almandine; Prp, pyrope; Grs, grsossular; Parg, pargasite; Fe Pa, ferro-pargasite; Tsc, tschermakite; Ab, albite (low); An, anorthite; Qtz, beta-quartz.
[b] Phases used in calculation; Fsl, ferrosilite; En, orthoenstatite; Hd, hedenbergite; Di, diopside; Ab, albite; An, anorthite; Parg, pargasite; Qtz, beta-quartz; W, water.

ternary feldspar solvus is useful in estimating peak metamorphic conditions. Determination of UHT temperature in mafic granulites requires reintegration of antiperthite to yield original hypersolvus feldspar compositions which, in turn, provide peak metamorphic temperatures using feldspar solvus geothermometry. We used back-scattered electron images to calculate the modal proportion of host and lamellae feldspar in the antiperthite. These data were then combined with quantitative analysis of individual spots on host and lamellae to obtain a reintegrated feldspar composition. Temperatures were determined graphically with the SOLVCALC 2.0 program of Wen and Nekvasil (1994), using the feldspar solution model of Fuhrman and Lindsley (1988) to calculate the position of isotherms. Consistent ultra high temperatures of ≥ 950 °C conditions were deduced by this method (Fig. 9).

8. Discussion

The close-to-peak temperatures of >900 °C obtained for the mafic granulites from the Panrimalai area are compatible with temperatures (900–1000 °C) reported for Mg–Al granulites from the adjoining Palni hills (Raith et al., 1997). The near-isothermal segment of P–T path encompasses up to 4.5 kbar decompression from 9 kbar (Fig. 10b). The metamorphic P–T conditions recorded in the Panrimalai area from the present study and the adjoining regions (e.g. Kiranur: Lal et al., 1984; Ganguvarpatti: Mohan and Windley, 1993; Usilampatti: Subba Rao et al., 1995; Kodaikanal: Mohan et al., 1996; Prakash, 1999b; Perumalmalai: Raith et al., 1997; Kambam: Anto et al., 1997) point strongly to a decompressional history (Fig. 11). This stage of near-isothermal decompression (ITD) implies ascent of the granulites possibly due to a collisional tectonic setting (England and Thompson, 1984; Harley, 1989). In the mafic granulites of the present study, there is evidence for preservation of near-peak UHT metamorphic conditions following the prograde arm. Well-established clockwise P–T paths documented in the literature from SGT (Kiranur: Lal et al., 1984; Ganguvarpatti: Mohan and Windley, 1993; Perumalmalai: Mohan et al., 1996; Raith et al., 1997) further substantiate a CW P–T path for the Panrimalai mafic granulites, consistent with crustal thickening followed by extensional collapse (Harley, 1989; Brown, 2002). Such a CW ITD P–T path is common to many mid-lower crustal granulite terrains, e.g. Gruf complex, Italian central Alps (Droop and Bucher-Nurminen, 1984), In Ouzzal, Algeria (Ouzegane and Boumaza, 1996), and Lützow-Holm Bay, East Antarctica (Motoyoshi and Ishikawa, 1997).

The P–T conditions of metamorphism further suggest that the Panrimalai mafic granulites were buried to depths of ca. 34 km. Beneath the exhumed granulite terrain in southernmost India, the geophysical observations suggest a crustal thickness of ca. 40 km (Radhakrishana et al., 2003). Thus Panrimalai mafic granulites represent exhumed lower crustal levels, an observation which is in accordance with the views of Bohlen and Mezger (1989) that many granulites represent exposed sections of mid-lower crustal resident material.

8.1. Timing and duration of metamorphism

The Madurai block is now believed to be involved in a major Pan-African tectonothermal event as indicated by U–Pb zircon data and Sm–Nd garnet-whole rock isochron data. U–Pb data on zircon overgrowths suggest an ancient high- grade thermal event close 1.85 Ga (Jayananda et al., 1995a). A charnockite sample from Kodaikanal massif define a Sm–Nd Gt-WR isochron age of 553±15 Ma (Jayananda et al., 1995b) for the near peak metamorphism, which is in conformity with an U–Pb zircon overgrowth age of 547±14 Ma obtained for a sample of metagranite (Bartlett et al., 1995). About 30 km northeast of Kodaikanal, another charnockite sample gave single zircon evaporation ages in the range of 650–560 Ma (Jayananda et al., 1995a). However, these zircons do not have any overgrowth or inherited cores.

These ages, therefore, could represent either zircon growth during magmatic crystallization of their protoliths or growth of new zircon during the Pan-African tectonothermal event. It appears that zircons in the original protoliths lost their earlier memory due to resetting of the U–Pb clock during the Pan-African tectonothermal event. Similar Pb-loss in zircons during Pan-African metamorphism have also been reported from Sri Lanka (Kröner et al., 1994), Madagascar (Paquatte et al., 1994) and East Antarctica (Shiraishi et al., 1994).

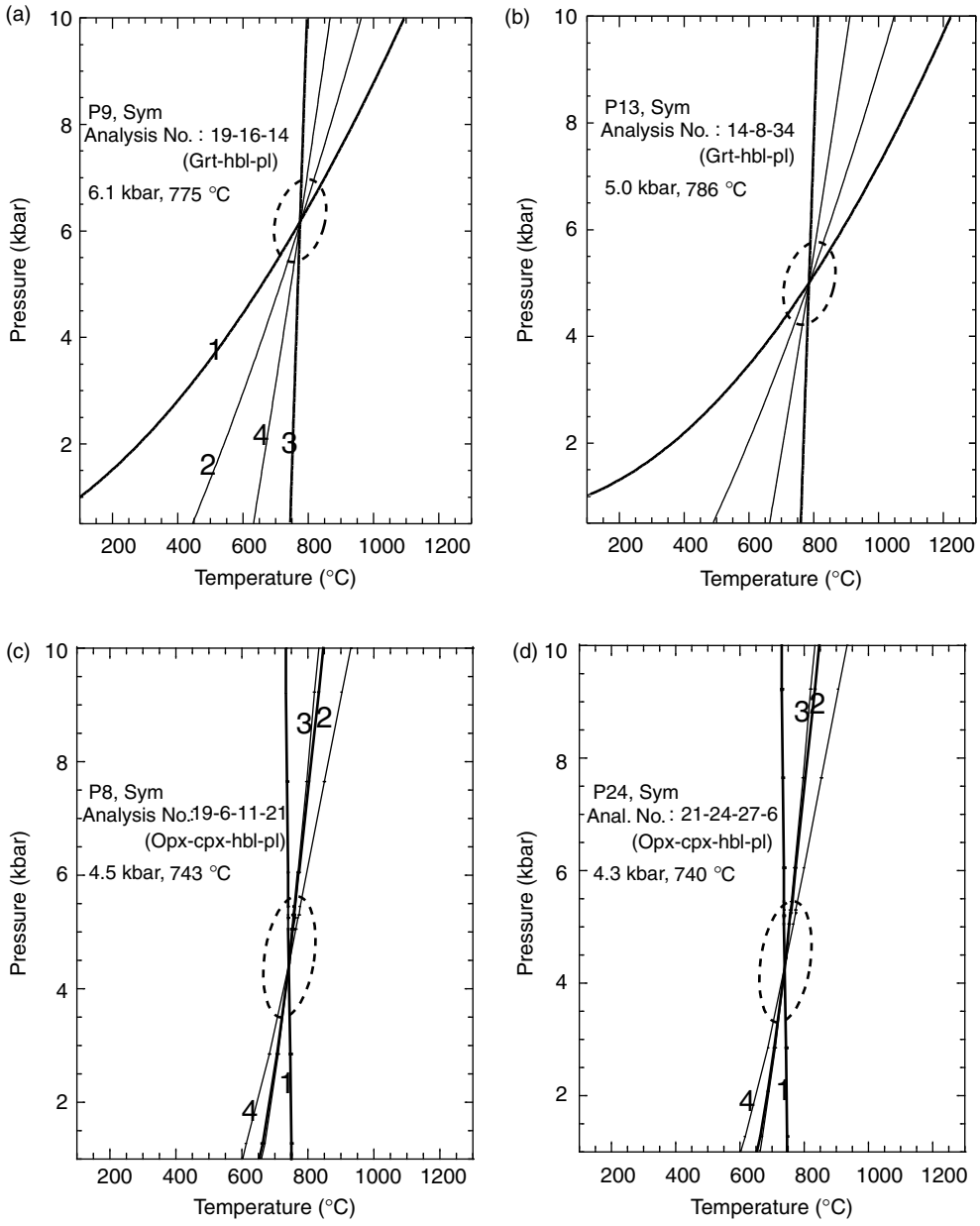


Fig. 8. TWQ (version 1.02) results for hornblende–plagioclase and hornblende–quartz symplectitic stages. The specific equilibria are listed in Table 4.

A Sm–Nd Gt-WR isochron for a two pyroxene granulite define an age of 459±19 Ma, which has been attributed to an isothermal decompression path, as these mafic granulites contain symplectitic assemblages of orthopyroxene + plagioclase around garnet. A Rb–Sr biotite cooling age of 425±55 Ma was also reported for the Madurai gneisses (Hansen et al., 1985). In summary, the time period from 459 to 425 Ma may represent the cooling and isothermal uplift path.

8.2. Evolution of magmatic protoliths

Geochronologic and isotopic studies have been recently initiated in the Madurai block. Some Nd model ages indicate that differentiation of crustal protoliths from depleted mantle occurred during 3.2–2.0 Ga (Harris et al., 1994; Brandon and Meen, 1995). On the contrary, single zircon evaporation ages, together with U–Pb zircon concordia, define ages ranging from 2.5 to 2.1 Ga for the magmatic crystallization of protoliths (Bartlett et al., 1995; Jayananda et al., 1995a). The analysed samples show a large variation in ϵNd values at 2.1 Ga forming two groups; one group characterized by high negative ϵNd values (−7.46 to −5.68 at 2.1 Ga), while the other group shows ϵNd values close to zero (−0.47 to + 1.5 at 2.1 Ga), suggesting derivation of magmatic protoliths from source regions with mixed contributions from depleted mantle as well as the ancient crust. In view of Sm/Nd fractions during intracrustal melting and granulite metamorphism, Nd model ages have little real meaning in that they neither

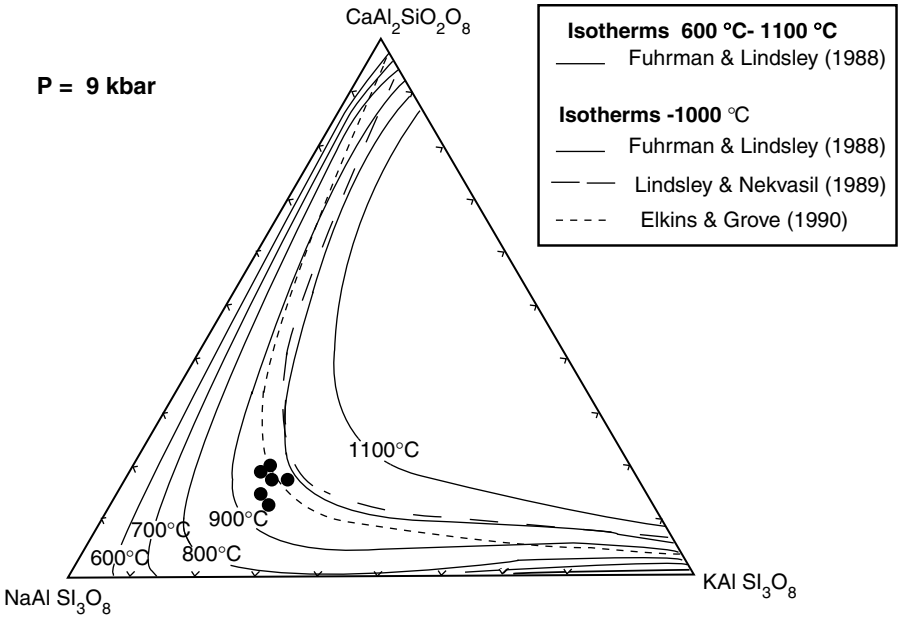


Fig. 9. Ternary plots of re-integrated feldspar compositions for mafic granulites along with the solvus curves calculated at 9 kbar using the model of Fuhrman and Lindsley (1988) for 600–1100 °C, and those of Lindsley and Nekvasil (1989) and Elkins and Grove (1990) for 1000 °C. Small solid circles are plots of the analyzed points from samples P1 and P5.

reflect magmatic crystallization age nor the age of their crustal source. The apparent discrepancy between Nd isotope data and zircon ages indicate that continental crust in the Madurai block represents reworked ancient crust with significant contributions from depleted mantle (Jayananda and Peucat, 1996). Detailed geochemical data, particularly on trace elements, is needed for rocks from the Madurai block in order to discuss petrogenetic mechanisms involved in the genesis of magmatic protoliths of granulites.

9. Implications of Gondwana reconstruction

The study of dispersed mobile belts provides a record of the changing map patterns of Earth through time. The assembly and breakup of supercontinents within Gondwanaland has stirred a revolution for conceptual thinking on Precambrian mobile belts. UHT metamorphism of granulites stimulates curiosity over the possible existence of megacontinents and may provide evidence relevant to the reconstruction of supercontinents. UHT–ITD metamorphism is preserved at several widely dispersed localities in the Indo-Antarctic sector and offer key features in order to construct a model for their correlation.

Extensive structural and petrological investigations in conjunction with the geochronological database for East Antarctic high-grade granulites have demarcated distinct age provinces with exclusive tectonometamorphic histories. The four high- grade belts of the East Antarctic shield, viz., the Dronning Maud Land, Lützow-Holm Bay, Prydz Bay and Denman Glacier with distinct crustal evolution histories point to the fact that East Antarctica cannot be treated as a single unified crustal block within either East Gondwana or Rodinia until Pan-African tectonism (see review in Harley, 2003). A similar conclusive scenario is not well documented in the southern Indian shield, viz., SGT, Dharwar craton and the Eastern Ghats belt despite an extensive petrological database (Mohan, 2003, 2004). UHT localities from India–Srilanka–Antarctica record remarkably similar mineral assemblages and textural relationships (cf. Harley, 2003) that provide key features in order to compare the tectonometamorphic histories. Similarties in UHT metamorphism, tectonic styles and Neoproterozoic U–Pb ages suggest a common Pan-African tectonothermal evolution for the juxtaposition of southern India, Sri Lanka and Lützow-Holm Bay of Eastern Antarctica. Current researches provide strong evidence for UHT metamorphism in parts of the SGT (Raith et al., 1997; Nandakumar and Harley, 2000; Prakash and Arima, 2003; Tateishi et al., 2004; Prakash et al., 2006a), in the Highland series of Sri Lanka (Kriegsman and Schumacher, 1999) and in the Lützow-Holm complex (Motoyoshi and Ishikawa, 1997) of East Antarctica. In the given framework, the polymetamorphosed SGT, India, is vital for the Indo-Antarctic assembly. The polyphase tectonometamorphic evolution of SGT has gained support from isotopic studies carried out by Jayananda et al. (1995a,b) and Bartlett et al. (1998). Proterozoic emplacement of enderbitic intrusives in the Palni region, in addition to the Pan-African event recorded from Sm–Nd to U–Pb dating of garnet, monazite and metamorphic zircon undergrowths, indicate that the SGT was subjected to more than one metamorphic episode. Available geochronological data suggest that the last major thermal event in SGT took place during the late Pan-African orogeny, concident with the assembly of the Gondwana supercontinent (Santosh et al., 2003, and references therein). The Pan-African granulite metamorphism is

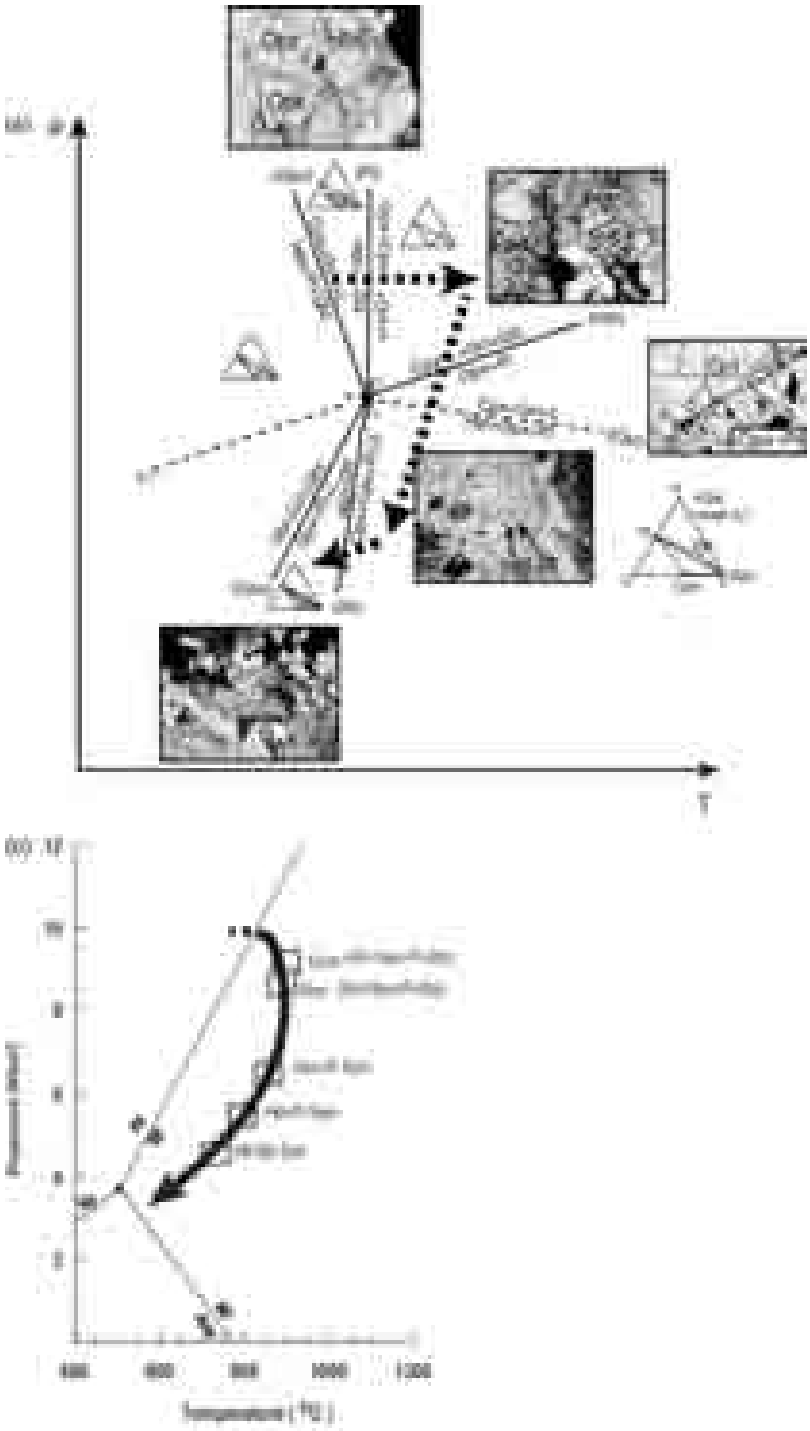


Fig. 10. (a) Petrogenetic grid for mafic granulites in the CaO–(FeO + MgO)–Al_2O_3–SiO_2–L (liquid) system after Pattison (2003). The topology in the divariant fields is shown in the ACF diagram with quartz and melt (L) as excess phases. Inferred PT path shown by the arrow. (b) Metamorphic *P–T* condition as defined by the core, rim and symplectite compositions in the mafic granulites from Panrimalai. Al_2SiO_5 stability relations from Hemingway et al. (1991). Proposed *P–T* path is shown by arrow in conjunction with relevant microstructural evidence.

equally well recognized in other terrains that made up part of the supercontinent.

U–Pb geochronological evidence from zircon within high-grade rocks from the Lützow-Holm Bay area (Shiraishi et al., 1994), East Antarctica, also indicate that the main granulite-facies event in this part of Antarctica is Pan-African (Harley, 2003 and the references therein). Thus, correlation of the granulite grade Pan-African event is evident by the rapid post-peak isothermal decompression path, extensive crustal melting and comparable UHT

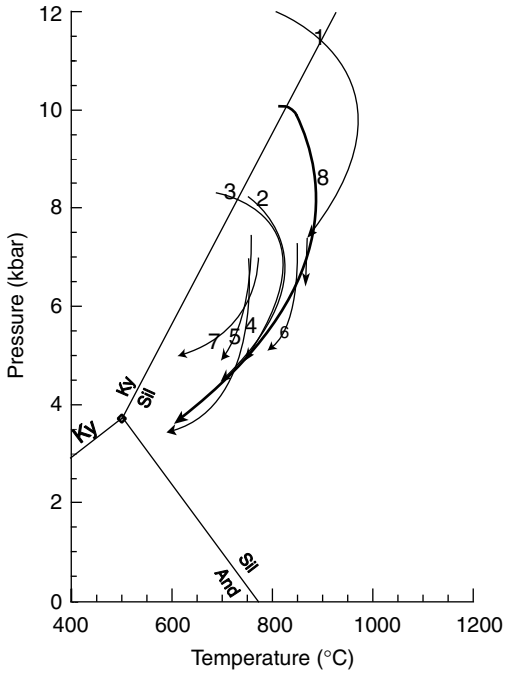


Fig. 11. *P–T* paths of granulites from Palni hill and selected adjoining areas. (1) Ultra-high temperature sapphirine granulites from Perumalmalai (Raith et al., 1997); (2) Sapphirine granulites from Ganguvarpatti (Mohan and Windley, 1993); (3) Sapphirine granulites from Kiranur (Lal et al., 1984); (4) Charnockites from Kodaikanal (Mohan et al., 1996); (5) Pelitic gneisses from Kodaikanal (Prakash, 1999b); (6) Sapphirine granulites from Kambam valley (Anto et al., 1997); (7) Pelitic gneisses from Usilampatti (Subba Rao et al., 1995); (8) Mafic granulites from Panrimalai (this study).

metamorphism preserved at several widely dispersed localities in the Antarctic–Indian sector. Correlation models undertaken by other workers further strengthen the East Gondwana connection as the Pan-African activity extends from Madagascar (cf. De Wit et al., 2001; Markl et al., 2000), SGT (Jayananda et al., 1995a; Bartlett et al., 1998; Mohan and Jayananda, 1999; Santosh et al., 2003) and Sri Lanka (Baur et al., 1991; Kröner et al., 1994) to East Antarctica (Rogers et al., 1994; Brandon and Meen, 1995; Fitzsimons, 2000; Boger et al., 2001). However, for conclusive correlations within the Gondwana context, more geochronological and isotopic data are needed from the SGT.

10. Conclusions

Reaction textures in conjunction with mineral data suggest that garnet consuming reactions are preserved in mafic granulites, defining a drop from higher to lower pressures along a nearly isothermal decompression (ITD) path. The Panrimalai mafic granulites document a clockwise decompression *P–T* trajectory, consistent with crustal thickening followed by extensional collapse. A possible correlation of similar post-peak decompressional textures and comparable UHT conditions in high-grade granulites in southern India, Sri Lanka, Madagascar and East Antarctica support the possibility that thses continents share a common metamorphic *P–T* history and formed an integral part of the East Gondwana framework. Future isotopic data from this region would provide important constraints on the exhumation history of the SGT.

Acknowledgements

This work has been possible through DST grant (SR/FTP/ES-27/2003) to DP. We are grateful to R. Berman for making his TWQ program available to us. Two samples were analyzed for colour-coded compositional mapping at NIPR, Japan. The authors thank K. Shiraishi for the help extended during this facility and T. Usuki for overall support. Thanks are due to Profs S.L. Harley, G. Clark and N. Daczko for their comments on certain aspects of this work. The authors thank Prof. J.C. Schumacher and Prof. Y. Motoyoshi for constructive comments that led to substantial improvement in the manuscript.

References

Anto, K.F., Janardhan, A.S., Sivasubramanian, P., 1997. A new sapphirine occurrence from Kambam valley, Tamil Nadu and its possible relation to the Pan-African tectonothermal event. Current Science 73, 792–796.

Aranovich, L.Y., Podlesskii, K.K., 1989. Geothermobarometry of high grade metapelites: simultaneously operating reactions. In: Cliff, R.A., Yardley, B.W.D., Daly, J.S. (Eds.), Evolution of Metamorphic Belts, vol. 43. Blackwell, Oxford, pp. 45–61 (Geological Society Special publication).

Attoh, K., 1998. Models for orthopyroxene–plagioclase and other corona reactions in metanorites, Dahomeyide orogen, West Africa. Journal of Metamorphic Geology 16, 345–362.

Bartlett, J.M., Harris, N.B.W., Hawkesworth, C.J., Santosh, M., 1995. New isotope constraints on crustal evolution of southern India and Pan-African metamorphism. Memoir Geological Society of India 34, 391–397.

Bartlett, J.M., Dougherty-Page, J.S., Harris, N.B.W., Hawkesworth, C.J., Santosh, M., 1998. The application of single zircon evaporation and model Nd ages to the interpretation of polymetamorphic terrains: an example from the proterozoic mobile belt of south India. Contributions to Mineralogy and Petrology 131, 181–195.

Baur, N., Kröner, A., Liew, T.C., Todt, W., Williams, I.S., Hofmann, A.W., 1991. U–Pb isotopic systematics from prograde and retrograde transition zones in high-grade orthogneisses, Sri Lanka. Journal of Geology 99, 527–545.

Berman, R.G., 1988. Internally consistent thermodynamic data for minerals in the system Na_2O–K_2O–CaO–MgO–FeO–Fe_2O_3–Al_2O_3–SiO_2–TiO_2–H_2O–CO_2. Journal of Petrology 29, 445–522.

Berman, R.G., 1990. Mixing properties of Ca–Mg–Fe–Mn garnets. American Mineralogist 75, 328–344.

Berman, R.G., 1991. Thermobarometry using multi-equilibrium calculations: a new technique with petrological applications. Canadian Mineralogist 29, 833–855.

Berman, R.G., Aranovich, L.Y., 1996. Optimized standard state and mixing properties of minerals: I. model calibration for olivine, orthopyroxene, cordierite, garnet, and ilmenite in the system FeO–MgO–CaO–Al_2O_3–TiO_2–SiO_2. Contributions to Mineralogy and Petrology 126, 1–24.

Berman, R.G., Aranovich, L.Y., Pattison, D.R.M., 1995. Reassessment of garnet–clinopyroxene Fe–Mg exchange thermometer: II. Thermodynamic analysis. Contributions to Mineralogy and Petrology 119, 30–42.

Bhattacharya, A., Krishnakumar, K.R., Raith, M., Sen, S.K., 1991. An improved set of *a–x* parameter for Fe–Mg–Ca garnet and refinement of the Opx–Gt thermometer and the Opx–Gt–Plag–Qtz barometer. Journal of Petrology 32, 629–656.

Bhowmik, S.K., Roy, A., 2003. Garnetiferous metabasites from the sausar mobile belt: petrology, *P–T* path and implications for the tectonothermal evolution of central Indian tectonic zone. Journal of Petrology 44, 387–420.

Boger, S.D., Wilson, C.J.L., Fanning, C.M., 2001. Early palaeozoic tectonism within the east Antarctic craton; the final suture between east and west Gondwana? Geology 29, 463–466.

Bohlen, S.R., Mezger, K., 1989. Origin of granulite terrains and the formation of lowermost continental crust. Science 244, 326–329.

Bohlen, S.R., Wall, V.J., Boettcher, A.L., 1983. Experimental investigation and application of garnet granulite equilibria. Contributions to Mineralogy and Petrology 83, 52–61.

Brandon, A.D., Meen, J.K., 1995. Nd isotopic evidence for the position of southernmost Indian terranes within East Gondwana. Precambrian Research 70, 269–280.

Brodie, K.H., 1995. The development of orientated symplectites during deformation. Journal of Metamorphic Geology 13, 499–508.

Brown, M., 2002. Retrograde processes in migmatites and granulites revisited. Journal of Metamorphic Geology 20, 25–40.

Dasgupta, S., Sengupta, P., Mondal, A., Fukuoka, M., 1993. Mineral chemistry and reaction textures in metabasites from the Eastern Ghats belt, India and their implications. Mineralogical Magazine 57, 113–120.

De Wit, M.J., Bowring, S.A., Ashwal, L.A., Randrianasolo, L.G., Morel, V.P.I., Rambeloson, R.A., 2001. Age and tectonic evolution of neoproterozoic ductile shear zones in south-western Madagascar, with implications for Gondwana studies. Tectonics 20, 1–45.

Droop, G.T.R., 1987. A general equation for estimating Fe^{3+} concentrations in ferromagnesian silicate and oxides from microprobe analyses, using stoichiometric criteria. Mineralogical Magazine 51, 431–435.

Droop, G.T.R., Bucher-Nurminen, K., 1984. Reaction textures and metamorphic evolution of sapphirine bearing granulites from the Gruf complex, Italian central Alps. Journal of Petrology 25, 766–803.

Eckert Jr, J.O., Newton, R.C., Kleppa, O.J., 1991. ΔH of reaction and recalibration of garnet–pyroxene–plagioclase–quartz geobarometers in the CMAS system by solution calorimetry of stoichiometric mineral mixes. American Mineralogist 76, 148–160.

Elkins, L.T., Grove, T.L., 1990. Ternary feldspar experiments and thermodynamic models. American Mineralogist 75, 544–559.

Ellis, D.J., Green, D.H., 1979. An experimental study of the effect of Ca upon garnet–clinopyroxene-exchange equilibria. Contributions to Mineralogy and Petrology 71, 13–22.

England, P.C., Thompson, A.B., 1984. Pressure–temperature–time paths of regional metamorphism, part II: heat transfer during the evolution of regions of thickened contionental crust. Journal of Petrology 25, 894–928.

Fitzsimons, I.C.W., 2000. Grenville-age basement provinces in East Antarctica: evidence for three separate collisional orogens. Geology 28, 879–882.

Frost, B.R., Chacko, T., 1989. The granulite uncertainty principle: limitations on thermobarometry in granulites. Journal of Geology 97, 435–450.

Fuhrman, M.L., Lindsley, D.H., 1988. Ternary–feldspar modeling and thermometry. American Mineralogist 73, 201–216.

Ganguly, J., 1979. Garnet and clinopyroxene solid solutions and geothermometry based on Fe–Mg distribution coefficients. Geochimica et Cosmochimica Acta 43, 1021–1029.

Ganguly, J., Hensen, B.J., Cheng, W., 2001. Reaction texture and Fe–Mg zoning in granulite garnet from Søstrene island, Antarctica: modeling and constraint on the time scale of metamorphism during the Pan-African collisional event. Proceedings of the Indian Academy of Sciences 110, 305–312.

Grew, E.S., 1984. Note on sapphirine and sillimanite + orthopyroxene from Panrimalai, Maduari District, Tamil Nadu. Journal of the Geological Society of India 25, 116–119.

Hansen, E.C., Hickman, M.H., Grant, N.K., Newton, R.C., 1985. Pan-African age of peninsular gneiss near Madurai, South India. American Geophysical Union (EOS) 664, 19–420.

Harley, S.L., 1984. An experimental study of the partitioning of Fe and Mg between garnet and orthopyroxene. Contributions to Mineralogy and Petrology 86, 359–373.

Harley, S.L., 1988. Proteropzoic granulites from the rauer group, east Antarctica. I. Decompressional pressure–temperature paths deduced from mafic and felsic gneisses. Journal of Petrology 29, 1059–1095.

Harley, S.L., 1989. The origins of granulites: a metamorphic perspective. Geological Magazine 126, 215–247.

Harley, S.L., 1998. On the occurrence and characterization of ultrahigh-temperature crustal metamorphism. In: Treloar, P.J., O'Brien, P.J. (Eds.), What Drives Metamorphism and Metamorphic Reactions?, vol 138. Geological Society, London, pp. 81–107 (Special publication).

Harley, S.L., 2003. Archaean–cambrian crustal development of East Antarctica: metamorphic characteristics and tectonic implications. In: Yoshida, M., Windley, B.F., Dasgupta, S. (Eds.), Proterozoic East Gondwana: Supercontinent Assembly and Breakup, vol. 206. Geological Society, London, pp. 203–230.

Harris, N.B.W., Holt, R.W., Drury, S.A., 1994. Crustal evolution in South India: constraints from Nd isotopes. Journal of Geology 102, 139–150.

Hemingway, B.S., Robie, R.A., Evans, J.T., Kerrick, D.M., 1991. Heat capacities and entropies of sillimanite, fibrolite, andalusite, kyanite, and quartz and the Al_2SiO_5 phase diagram. American Mineralogist 76, 1597–1613.

Hokada, T., 2001. Feldspar thermometry in ultrahigh-temperature metamorphic rocks: evidence of crustal metamorphism attaining 1100 °C in the Archean Napier complex, East Antarctica. American Mineralogist 86, 932–938.

Holtta, P., Paavola, J., 2000. *P–T–t* development of archaean granulites in Varpaisjarvi, Central Finland, I. Effect of multiple metamorphism on the reaction history of mafic rocks. Lithos 50, 97–120.

Jayananda, M., Peucat, J.-J., 1996. Geochronological framework of southern India. In: Santosh, M., Yoshida, M., (Eds.), Gondwana Research Memoir No.: Th Archean and Proterozoic Terrains in Southern India within East Gondwana, pp. 53–75.

Jayananda, M., Janardhan, A.S., Sivasubramanian, P., Peucat, J.J., 1995a. Geochronology and isotopic constraints on granulite formation in the Kodaikanal area, southern India. Memoir Geological Society of India 34, 373–390.

Jayananda, M., Martin, H., Peucat, J.J., Mahabaleswar, B., 1995b. Late archaean crust-mantle interactions: geochemistry of LREE enriched mantle derive magmas: example of the closepet batholith. Contributions to Mineralogy and Petrology 119, 314–329.

Jones, K.A., Escher, J.C., 2002. Near-isothermal decompression within a clockwise P-T evolution recorded in migmatitic mafic granulites from clavering Ø, NE Greenland: implications for the evolution of the Caledonides. Journal of Metamorphic Geology 20, 365–378.

Kohn, M.J., Spear, F.S., 1989. Empirical calibration of geobarometers for the assemblage garnet–hornblende–plagioclase–quartz. American Mineralogist 74, 77–84.

Kohn, M.J., Spear, F.S., 2000. Retrograde net transfer reaction insurance for pressure–temperature estimates. Geology 28, 1127–1130.

Koshimoto, S., Tsunogae, T., Santosh, M., 2004. Sapphirine and corundum bearing ultrahigh temperature rocks from the palghat–cauvery shear system, Southern India. Journal of Mineralogical and Petrological Sciences 99, 298–310.

Kretz, R., 1983. Symbols for rock-forming minerals. American Mineralogist 68, 277–279.

Kriegsman, L.M., Schumacher, J., 1999. Petrology of sapphirine-bearing and associated granulites from central Sri Lanka. Journal of Petrology 40, 1211–1239.

Kröner, A., Jaeckel, P., Williams, I.S.M., 1994. Pb-loss patterns in zircons from high grade metamorphic terrain as revealed by different dating method: U–Pb and Pb–Pb age for igneous and metamorphic rocks from northern Sri Lanka. Precambrian Research 66, 151–181.

Lal, R.K., 1993. Internally consistent recalibrations of mineral equilibria geothermobarometry involving garnet–orthopyroxene–plagioclase–quartz assemblages and their application to the South Indian granulites. Journal of Metamorphic Geology 11, 855–866.

Lal, R.K., Ackermand, D., Raith, M., Raase, P., Seifert, F., 1984. Sapphirine-bearing assemblages from Kiranur, southern India: a study of chemographic relationships in the Na_2O–FeO–MgO–Al_2O_3–SiO_2–H_2O system. Neus Jahrbuch für Mineralogische Abhandlungen 150, 121–152.

Leake, B.E., Woolley, A.R., Arps, C.A.E.S., et al., 1997. Nomenclature in amphiboles: report of the subcommittee on amphiboles of the international mineralogical association commission on new mineral and mineral names. Mineralogical Magazine 61, 295–321.

Lee, H.Y., Ganguly, J., 1988. Equilibrium compositions of coexisting garnet and orthopyroxene: experimental determinations in the system FeO–MgO–Al_2O_3–SiO_2. Journal of Petrology 29, 93–113.

Lindsley, D.H., Nekvasil, H., 1989. A ternary feldspar model for all reasons. EOS, Transactions American Geophysical Union 70, 506.

Madar, U.K., Percial, J.A., Berman, R.G., 1994. Thermobarometry of garnet–clinopyroxene–hornblende granulite from the kapuskasing structural zone. Canadian Journal of Earth Sciences 31, 1134–1145.

Markl, G., Bäuerle, J., Grujic, D., 2000. Metamorphic evolution of Pan-African granulite facies metapelites from southern Madagascar. Precambrian Research 102, 47–68.

Mengel, F., Rivers, T., 1991. Decompression reactions and *P–T* conditions in high-grade rocks, Northern Labrador: *P–T–t* paths from individual samples and implications for early proterozoic tectonic evolution. Journal of Petrology 32, 139–167.

Moecher, D.P., Anovitz, L.M., Essene, E.J., 1988. Calculation of clinopyroxene–garnet–plagioclase–quartz geobarometers and application to high-grade metamorphic rocks. Contributions to Mineralogy and Petrology 100, 92–106.

Mohan, A. (Eds.), 2003. Milestones in Petrology and future perspectives. Journal of the Geological Society of India, Memoir, 52, 471.

Mohan, A., 2004. Metamorphic petrology—III: eastern Ghats and southern Granulite Terrane. In: Singhvi, A.K., Bhattacharya A. (Eds.), Glimpses of Geoscience Research in India, INSA Report 1999–2004, pp. 92–94.

Mohan, A., Jayananda, M., 1999. Metamorphism and isotopic evolution of granulites of southern India: reference to neoproterozoic crustal evolution. Gondwana Research 2, 251–262.

Mohan, A., Lal, R.K., 1986. Genesis of silica-deficient granulites from Ganguvarpatti Madurai district, Tamil Nadu. Quaternary Journal of the Geological, Mineralogical and Metallurgical Society of India 58, 99–110.

Mohan, A., Windley, B.F., 1993. Crustal trajectory of sapphirine-bearing granulites from Ganguvarpatti, South India: evidence for an isothermal decompression path. Journal of Metamorphic Geology 11, 867–878.

Mohan, A., Ackermand, D., Lal, R.K., 1985. Granulites of Ganguvarpatti, Madurai, Tamil Nadu. Indian Journal of Earth Sciences 12, 255–278.

Mohan, A., Prakash, D., Motoyoshi, Y., 1996. Decompressional *P–T* history in the sapphirine-bearing granulites from Kodaikanal, southern India. Journal of Asian Earth Sciences 14, 231–243.

Mohan, A., Sharma, I.N., Singh, P.K., 2005. UHT metamorphism and continental orogenic belts. In: Thomas, H. (Ed.), Metamorphism and Crustal Evolution. Atlantic Publishers, pp. 314–335.

Motoyoshi, Y., Ishikawa, M., 1997. Metamorphic and structural evolution of granulites from Rundvagshetta, Lutzow-Holm Bay, East Antarctica. In: The Antarctic Region: Geological Evolution and Processes, Terra Antarctica Publications, pp. 100–110.

Nandakumar, V., Harley, S.L., 2000. A reappraisal of the pressure–temperature path of granulites from the Kerala Khondalite belt, southern India. Journal of Geology 108, 687–703.

Newton, R.C., 1983. Geobarometry of high-grade metamorphic rocks. American Journal of Science 283-A, 1–28.

Norlander, B.H., Whitney, D.L., Teyssier, C., Vanderhaeghe, O., 2002. Partial melting and decompression of the thor-odin dome, shuswap metamorphic core complex, Canadian cordillera. Lithos 61, 103–125.

Ouzegane, K., Boumaza, S., 1996. An example of ultrahigh-temperature metamorphism: orthopyroxene–sillimanite–garnet, sapphirine–quartz and spinel–quartz parageneses in Al–Mg granulites from In Hihaou, In Ouzzal, Hoggar. Journal of Metamorphic Geology 14, 693–708.

Ouzegane, K., Bendaoud, A., Kienast, J.R., Touret, J.L.R., 2001. Pressure–temperature–fluid evolution in Eburnean metabasites and metapelites from Tamanrasset (Hoggar, Algeria). Journal of Geology 109, 247–263.

Paquatte, J.-L., Nedlac, A., Moine, B., Rakotondrazafy, R., 1994. U–Pb zircon evaporation and Sm–Nd isotope study of a granulite domain in SE Madagascar. Journal of Geology 102, 523–538.

Pattison, D.R.M., 2003. Petrogenetic significance of orthopyroxene-free garnet + clinopyroxene + plagioclase±quartz bearing metabasites with respect to the amphibolite and granulite facies. Journal of Metamorphic Geology 21, 21–34.

Pattison, D.R.M., Newton, R.C., 1989. Reversed experimental calibration of the garnet–clinopyroxene Fe–Mg exchange thermometer. Contributions to Mineralogy and Petrology 101, 87–103.

Perkins III, D., Chipera, S.J., 1985. Garnet–orthopyroxene–plagioclase–quartz barometry: refinement and application to the english river subprovince and the minnesota river valley. Contributions to Mineralogy and Petrology 89, 69–80.

Prakash, D., 1999a. Petrology of the basic granulites from Kodaikanal, South India. Gondwana Research 2, 95–104.

Prakash, D., 1999b. Cordierite-bearing gneisses from Kodaikanal, South India: textural relationship and *P–T* conditions. Journal of the Geological Society of India 54, 347–358.

Prakash, D., Arima, M., 2003. High-temperature dehydration melting and decompressive textures in Mg–Al granulites from the Palni hills, South India. Polar Geosciences 16, 149–175.

Prakash, D., Arima, M., Mohan A., in press-a. UHT metamorphism in the Palni Hills, South India: insights from feldspar thermometry and phase equilibria. International Geology Review.

Prakash, D., Arima, M., Mohan A., in press-b. Colour-coded compositional mapping of orthopyroxene–plagioclase symplectites in mafic granulites from Panrimalai, South India, The Journal of Geological Society of India.

Radhakrishana, M., Kurian, P.J., Nambiar, C.G., Murty, B.V.S., 2003. Nature of the crust below southern granulite terrain (SGT) of Peninsular India across the Barvali shear zone based on analysis of gravity data. Precambrian Research 124, 21–40.

Raith, M., Karmakar, S., Brown, M., 1997. Ultrahigh-temperature metamorphism and multi-stage decompressional evolution of sapphirine granulites from the Palni hill ranges, Southern India. Journal of Metamorphic Geology 15, 379–399.

Ravindra Kumar, G.R., Chacko, T., 1994. Geothermobarometry of mafic granulites and metapelite from the Palghat gap, South India: petrological evidence for isothermal uplift and rapid cooling. Journal of Metamorphic Geology 12, 479–492.

Robinson, P., Spear, F.S., Schumacher, J.C., Laird, J., Klein, C., Evana, B.W., Doolan, B.L., 1982. Phase relations of metamorphic amphiboles: natural occurrence and theory. In: Veblen, D.R., Ribbe, P.H. (Eds.), Amphiboles: Petrology and Experimental Phase Relations, Reviews in Mineralogy, vol. 9B. Mineralogical Society of America, pp. 1–227.

Rogers, J.J.W., Unrug, R., Sultan, M., 1994. Tectonic assembly of Gondwana. Journal of Geodynamics 19, 1–34.

Rotzler, J., Romer, R.L., 2001. *P–T–t* evolution of ultrahigh-temperature granulites from the saxon granulite massif, Germany. part I: petrology. Journal of Petrology 42, 1995–2013.

Sajeev, K., Osanai, Y., Santosh, M., 2004. Ultrahigh-temperature metamorphism followed by two-stage decompression of garnet-orthopyroxene-sillimanite granulites from Ganguvarpatti, Madurai block, southern India. Contribution to Mineralogy and Petrology 148, 29–46.

Santosh, M., Yokoyama, K., Biju-Sekhar, S., Rogers, J.J.W., 2003. Multiple tectonothermal events in the granulite blocks of southern India revealed from EPMA dating: implications on the history of supercontinents. Gondwana Research 6, 29–63.

Sen, S.K., Bhattacharya, A., 1984. An orthopyroxene–garnet geothrmometer and its application to Madras charnockites. Contributions to Mineralogy and Petrology 88, 64–71.

Shiraishi, K., Ellis, D.J., Hiroi, Y., Fanning, C.M., Motoyoshi, Y., Nakai, Y., 1994. Cambrian orogeneic belt in east Antarctica and Sri Lanka: implications for Gondwana assembly. Journal of Geology 102, 47–65.

Sriramguru, K., Janardhan, A.S., Basava, S., Basavalingu, B., 2002. Prismatine and sapphirine bearing assemblages from Rajapalaiyam area, Tamil Nadu: origin and metamorphic history. The Journal of Geological society of India 59, 103–112.

Subba Rao, D.V., Nirmalcharan, S., Narayana, B.L., Naqvi, S.M., 1995. Symplectites in high-grade pelitic gneisses of Usilampatti, Tamil Nadu: *P–T* conditions and geochemistry. Journal of the Geological Society of India 46, 37–45.

Tamashiro, T., Santosh, M., Sajeev, K., Morimoto, T., Tsunogae, T., 2004. Multistage orthopyroxene formation in ultrahigh-temperature granulites of Ganguvarpatti, southern India: implications for complex metamorphic evolution during Gondwana assembly. Journal of Mineralogical and Petrological Sciences 99, 279–297.

Tateishi, K., Tsunogae, T., Santosh, M., Janardhan, A.S., 2004. First report of Sapphirine + Quartz assemblage from southern India: implications for ultrahigh-temperature metamorphism. Gondwana Research 7, 899–912.

Thost, D.E., Hensen, B.J., Motoyoshi, Y., 1991. Two-stage decompression in garnet-bearing mafic granulites from Søstrene Island, Prydz Bay, East Antarctica. Journal of Metamorphic Geology 9, 245–256.

Tsunogae, T., Santosh, M., 2003. Sapphirine and corundum-bearing granulites from Karur, Madurai block, Southern India. Gondwana Research 6, 925–930.

Wen, S., Nekvasil, H., 1994. SOLVCALC: An interactive graphics program package for calculating the ternary feldspar solvus and for two feldspar geothermometry. Computers and Geosciences 20, 1025–1040.

Yoshimura, Y., Motoyoshi, Y., Grew, E.S., Miyamoto, T., Carson, C.J., Dunkley, D.J., 2000. Ultrahigh-temperature metamorphic rocks from Howard hills in the Napier complex, East Antarctica. Polar Geosciences 13, 60–85.

Zhao, G., Wilde, S.A., Cawood, P.A., Lu, L.Z., 2000. Petrology and *P–T* path of the Fuping mafic granulites: implications for tectonic evolution of the central zone of the North China craton. Journal of Metamorphic Geology 18, 375–391.

Zhao, G., Cawood, P.A., Wilde, S.A., Lu, L.Z., 2001. High-pressure granulites (Retrograded Eclogites) from the Hengshan complex, North China craton: petrology and tectonic implications. Journal of Petrology 42, 1141–1170.